An analysis of the relationships between subthreshold electrical properties and excitability in skeletal muscle

Thomas H. Pedersen,[1,2] Christopher L.-H. Huang,[1] and James A. Fraser[1]

[1]Physiological Laboratory, University of Cambridge, Cambridge CB2 3EG, England, UK
[2]Department of Physiology and Biophysics, Aarhus University, 8000 Aarhus, Denmark

Skeletal muscle activation requires action potential (AP) initiation followed by its sarcolemmal propagation and tubular excitation to trigger Ca^{2+} release and contraction. Recent studies demonstrate that ion channels underlying the resting membrane conductance (G_M) of fast-twitch mammalian muscle fibers are highly regulated during muscle activity. Thus, onset of activity reduces G_M, whereas prolonged activity can markedly elevate G_M. Although these observations implicate G_M regulation in control of muscle excitability, classical theoretical studies in unmyelinated axons predict little influence of G_M on membrane excitability. However, surface membrane morphologies differ markedly between un-myelinated axons and muscle fibers, predominantly because of the tubular (t)-system of muscle fibers. This study develops a linear circuit model of mammalian muscle fiber and uses this to assess the role of subthreshold electrical properties, including G_M changes during muscle activity, for AP initiation, AP propagation, and t-system excitation. Experimental observations of frequency-dependent length constant and membrane-phase properties in fast-twitch rat fibers could only be replicated by models that included t-system luminal resistances. Having quantified these resistances, the resulting models showed enhanced conduction velocity of passive current flow also implicating elevated AP propagation velocity. Furthermore, the resistances filter passive currents such that higher frequency current components would determine sarcolemma AP conduction velocity, whereas lower frequency components excite t-system APs. Because G_M modulation affects only the low-frequency membrane impedance, the G_M changes in active muscle would predominantly affect neuromuscular transmission and low-frequency t-system excitation while exerting little influence on the high-frequency process of sarcolemmal AP propagation. This physiological role of G_M regulation was increased by high Cl^- permeability, as in muscle endplate regions, and by increased extracellular $[K^+]$, as observed in working muscle. Thus, reduced G_M at the onset of exercise would enhance t-system excitation and neuromuscular transmission, whereas elevated G_M after sustained activity would inhibit these processes and thereby accentuate muscle fatigue.

The Journal of General Physiology

INTRODUCTION

Skeletal muscle excitation–contraction coupling involves three successive electrophysiological processes in different surface membrane regions. Transmitter release at the neuromuscular junction first initiates electrotonic endplate potentials that in turn trigger the sarcolemmal action potential (AP). This propagates along the sarcolemma, in turn triggering APs in the transverse tubular (t)-system membrane that activate voltage sensors in the t-system membrane, thereby eliciting release of the intracellularly stored Ca^{2+} that triggers the contraction. All of these electrophysiological processes involve passive depolarization of initially resting sink membrane by local circuit currents generated by voltage gradients between an active source membrane region and the nearby resting sink membrane region. This passive depolarization then excites APs in the sink region and thereby converts it into a source region for further AP propagation (Hodgkin, 1937; Adrian and Peachey, 1973; Huang and Peachey, 1992). The effectiveness of this process depends on how the magnitude and time course of this intracellular current flow interacts with, that is, matches, the passive electrical properties of the initially quiescent membrane in the sink membrane region.

Recent studies report that the resting membrane conductance (G_M) of skeletal muscle fibers is markedly regulated during activity. Thus, in rat extensor digitorum longus (EDL) fast-twitch muscle fibers, the onset of AP firing is associated with ClC-1 Cl^- channel inhibition mediated by PKC that reduces G_M to ~40% of its resting level. However, after prolonged AP firing, G_M quickly and reversibly rises to about five times its resting level because of activation of both ClC-1 channels and K_{ATP} channels (Pedersen et al., 2009a,b).

Several previous observations shed light on the functional consequences of such G_M alterations for muscle excitability. First, Cl^- channel inhibition produced by

Correspondence to Thomas H. Pedersen: thp@fi.au.dk

Abbreviations used in this paper: AP, action potential; BTS, *N*-benzyl-*p*-toluene sulphonamide; DC, direct–current; EDL, extensor digitorum longus; G_M, resting membrane conductance; RC, resistance–capacitance.

© 2011 Pedersen et al. This article is distributed under the terms of an Attribution–Noncommercial–Share Alike–No Mirror Sites license for the first six months after the publication date (see http://www.rupress.org/terms). After six months it is available under a Creative Commons License (Attribution–Noncommercial–Share Alike 3.0 Unported license, as described at http://creativecommons.org/licenses/by-nc-sa/3.0/).

The Rockefeller University Press $30.00
J. Gen. Physiol. Vol. 138 No. 1 73–93
www.jgp.org/cgi/doi/10.1085/jgp.201010510

acidosis, PKC activation, or directly using 9-AC caused a pronounced recovery of excitability and force production in muscle depolarized by elevated extracellular K^+ (Nielsen et al., 2001; Pedersen et al., 2005, 2009b). Second, loss of ClC-1 channel function leads to the hyperexcitability observed in patients suffering from myotonia congenita (McComas and Mrozek, 1968; Bryant and Morales-Aguilera, 1971; Koch et al., 1992; Pusch, 2002). Third, metabolically poisoned frog muscles show a high G_M, and they are completely inexcitable despite the persistence of a normally polarized membrane potential (Fink and Lüttgau, 1976). Collectively, these observations suggest that G_M and muscle excitability are inversely related. In contrast, classical theoretical studies of the excitability of un-myelinated nerve fibers, which are fundamental for our understanding of membrane excitability, have generally concluded that G_M plays only a minor role in excitable cells (Hodgkin and Huxley, 1952; Noble, 1972). However, surface membrane morphologies differ substantially between un-myelinated nerve axons and muscle fibers because the extensive network of thin t-tubules with diameters around 120 nm constitute ~80% of the total surface area in muscle fibers (Gage and Eisenberg, 1969; Cullen et al., 1984; Dulhunty et al., 1984; Huang and Peachey, 1989; Stephenson, 2006). Thus, to evaluate the role of G_M for muscle excitability, it is important to take these different membrane morphologies into account and to distinguish between effects along the sarcolemma and effects in the t-system.

This study therefore sought to analyze and quantify the physiological role of G_M changes during AP firing in active muscle fibers for: (a) AP initiation, as occurs at the motor endplate; (b) sarcolemmal AP propagation; and (c) t-system excitation using a linear circuit model as appropriate for the subthreshold electrical processes that precede these nonlinear events (a–c) in the excitation–contraction coupling. Such analysis describes a linear system (the resting membrane) by relating the output of the system (changes in membrane potential) to the system inputs (electrotonic or circuit currents). Resting membranes of most excitable cells are well suited for such analysis within a narrow range of subthreshold membrane potentials. Although restrained to this subthreshold membrane potential range, this type of analysis has the benefit of providing clear physical insight into the system being explored through the analytical expressions that can be derived. In addition, the analysis was used to find an appropriate circuit model for the development of an iterative model of a muscle fiber in our companion study (see Fraser et al. in this issue) that includes nonlinear membrane phenomena necessary for testing the findings of the present study. Thus, we first develop an equivalent circuit model for the passive, linear membrane properties of mammalian muscle fibers and then use this model to explore the physiological significance of G_M changes for the processes (a–c).

Development of the model involved experimental two-electrode measurements of the membrane-impedance properties of rat EDL muscle fibers and comparison of the results to theoretical predictions from three different circuit models. This made it possible to determine and calibrate an appropriate cable circuit model for mammalian muscle fibers. These analyses showed that the t-system lumen of mammalian muscle exerts a significance resistance to current flow, resulting in transverse tubular luminal resistance that then must be included in the circuit model to obtain agreement between experiment and theoretical predictions, in accordance with observations in amphibian muscle (Falk and Fatt, 1964; Peachey, 1965; Schneider 1970; Adrian and Peachey, 1973; Valdiosera et al., 1974a,b,c; Eisenberg, 1983).

Analysis using this cable model of mammalian muscle fibers suggests that the t-system luminal resistance filters the circuit currents underlying AP propagation such that their higher frequency components are preferentially involved in sarcolemma AP propagation, thereby maximizing AP conduction velocity. In contrast, the t-system membrane is predominantly excited by the lower frequency components of the circuit currents appropriate for the activation of the slower kinetic processes involved in excitation–contraction coupling (Huang, 1988; Huang and Peachey, 1989). These effects of the t-system luminal resistance enhanced the physiological effects of the G_M changes observed in active muscle. Thus, modulation of G_M only influences the low frequency characteristics of the membrane impedance, such that it would predominantly affect neuromuscular transmission and t-system excitation. It has very little influence on the high frequency components of the circuit currents that determine the velocity of sarcolemmal AP propagation. However, under conditions where excitability is depressed, as with the increased extracellular $[K^+]$ encountered in working muscle, the high frequency content of the circuit currents is reduced and therefore the influence of G_M modulation is enhanced. It therefore seems likely that the rapid reduction in G_M at the start of muscle activity enhances neuromuscular transmission and t-system excitation, whereas the large increase in G_M after prolonged activity may significantly inhibit these processes and thereby contribute to muscle fatigue.

Theory

This study applied linear systems theory to evaluate the response of resting sink membrane to nonlinear electrical membrane properties in active source membrane regions, an analytical approach that allows specific attention to passive linear electrical membrane properties. A simple square current pulse was used as input function to mimic electrotonic currents similar to the endplate events that are responsible for AP initiation in vivo, and

an experimentally recorded AP was used to mimic the voltage gradient that drives the circuit currents responsible for AP propagation and t-system excitation. These inputs therefore allowed separate examination of the influence of t-system luminal resistance and G_M on sarcolemmal AP excitation and propagation and the subsequent t-system excitation. The outputs in the analysis were passive voltage responses that mimic the behavior of the sink membrane within the narrow subthreshold voltage range that shows a linear current–voltage relationship. Importantly, it is this voltage range through which the sink membrane potential traverses before becoming sufficiently depolarized to activate the voltage-gated Na^+ channels and to excite the AP.

These output voltages were obtained by performing convolutions of the input functions with transfer functions representing the linear electrical properties of the membranes under study. The latter were obtained analytically using linear cable theory for infinite cables that either omitted or included t-system luminal resistances. The mathematical procedures were markedly simplified by representing the functions and the circuits in the frequency domain. This used the property that convolutions in the time domain correspond to simple multiplications in the frequency domain (Bracewell, 1999). (For Fourier analysis of input and output, see Appendix 2.) Thus, in the frequency domain:

$$Output_{(x,f)} = Input_{(0,f)} H_{(x,f)}. \quad (1)$$

$H_{(x,f)}$ represents the transfer function. Note that Eq. 1 includes two independent variables: the term x represents the distance from the point of input application, and f is the frequency. Because the principle of superposition of different frequencies is central to linear systems theory, an expression was needed that describes how a sinusoidal current decays away from its point of application. It has been shown that the voltage response to a sinusoidal current decays exponentially with distance in an infinite cable structure (Falk and Fatt, 1964; Fig. 2 B). Thus, for input current, $I_{(0,f)}$,

$$V_{(x,f)} = Z_{in(f)} I_{(0,f)} \exp(-x/\lambda_{(f)}), \quad (2)$$

and for input voltage, $V_{(0,f)}$,

$$V_{(x,f)} = V_{(0,f)} \exp(-x/\lambda_{(f)}). \quad (3)$$

From superposition, the voltage response at a given distance along any cable structure to a waveform containing multiple frequencies can be determined by summing the voltage responses resulting from the individual frequencies. From Eqs. 2 and 3, the transfer functions for an input current, $H_{I(x,f)}$, and for an input voltage, $H_{V(x,f)}$, are therefore:

$$H_{I(x,f)} = Z_{in(f)} \exp(-x/\lambda_{(f)}), \quad (4)$$

and

$$H_{V(x,f)} = \exp(-x/\lambda_{(f)}). \quad (5)$$

Accordingly, the transfer function defined in Eq. 5 was used for convolution with the experimentally recorded AP, whereas the transfer function in Eq. 4, the transfer impedance, was used in the convolution with sinusoidal and square currents. The transfer functions are in turn determined by the frequency-dependent input impedance, $Z_{in(f)}$, and the frequency-dependent length constant, $\lambda_{(f)}$, given by:

$$Z_{in(f)} = \frac{\sqrt{Z_M R_i/2}}{2\pi a^{3/2}} \quad (6)$$

$$\lambda_{(f)} = \sqrt{Z_M a/2R_i}. \quad (7)$$

R_i represents intracellular resistivity, and a represents the fiber radius. The frequency dependence of $Z_{in(f)}$ and $\lambda_{(f)}$ arises from the frequency dependence of the equivalent impedance, $Z_{M(f)}$, of the circuit model under investigation (Fig. 2; for derivation, see Appendix 1). $Z_{M(f)}$ represents the sarcolemmal membrane and t-system elements, and r_i represents the intracellular axial resistance (Fig. 2, left panels).

Model cable structures

Predictions from the three different cable models were compared with experimental observations to determine the most appropriate linear cable model of mammalian muscle fibers for further analysis. The first of these models was the simple cable in which sarcolemmal and t-system membranes appeared as a single parallel resistance–capacitance (RC) component (Fig. 2 A, left), and the t-system luminal resistance was accordingly omitted. In contrast, in the second model for the lumped cable, an R_A term, set to 10 or 20% of the direct–current (DC) membrane impedance, was included at the opening of the t-system to separate sarcolemmal from t-system parallel RC components (Fig. 2 B, left). In the third model for a distributed cable, the t-system luminal resistance was distributed between 20 (n_1...n_{20}) shells that represent progressively deeper parts of the t-system. The thickness of each shell was the same, but their volumes were, consequently, inversely related to the depth of the t-system. The membrane capacitance in each t-system shell, $C_{M(t,n)}$, was distributed according to their volume with the total capacitance of the t-system being 80% of the total fiber capacitance. The membrane resistance for the different shells, $R_{M(t,n)}$, was determined by assuming the same time constant for all shell membranes ($\tau_{M(t)} = R_{M(t,n)} C_{M(t,n)}$) and the sarcolemma membrane ($\tau_{M,S} = R_{M,S} C_{M,S}$). Similarly, the product of the capacitance in each shell and the luminal resistance, $R_{L(t,n)}$,

for the shell was also assumed to be the same ($\tau_{L(t)} = R_{L(t,n)}C_{M(t,n)}$) for all shells. The resistance of the t-system lumina was based on a simple calculation of a resistance as being the product of its resistivity with the ratio of its length and its cross-sectional area. The diameter of a t-tubule in adult EDL muscle fibers, which were exclusively used in this study, has been shown to be ~120 nm (Cullen et al., 1984). The tortuosity factor of the t-system was 0.34 (Adrian et al., 1969a,b; Wallinga et al., 1999). For each of these models, determination of the $Z_{M(f)}$ term was required for the expressions for $H_{(x,f)}$ above (see Appendix 1).

When comparing the experimental observations to predictions from passive cable structures mimicking rat EDL muscle fibers, the models were initially adjusted to the experimentally determined values of fiber diameter, DC impedance, and total membrane capacitance in the particular fiber. In the convolution studies, when the appropriate model had been determined, the average values of a range of cable properties were used. EDL muscle fibers are >1 cm in length, and their fiber DC length constants are generally ~1 mm (Macdonald et al., 2005). All the modeling could accordingly be based on cable theory as applied to infinite linear cable structures. The internal resistivity, R_i, was obtained from previous reports (Albuquerque and Thesleff, 1968).

When comparing the responses between the different cable structures, the DC impedance and total membrane capacitance of unit surface membrane area were the same in all cable structures. In the cable structures with a t-system luminal resistance, 80% of the total membrane was assumed to be located in the t-system and the specific membrane resistance was assumed to be the same for the sarcolemma and the t-system membrane.

MATERIALS AND METHODS

Animal handling

The experiments used EDL muscles from 12-wk-old female Wistar rats weighing ~230 g. Animals were fed ad libitum and lived under 12:12-h light/dark conditions at a thermostat-controlled temperature at 21°C. All handling and killing of animals followed Danish welfare regulations. Muscles were incubated in standard Krebs-Ringer bicarbonate buffer (pH ~7.4 at 30°C) containing (in mM): 122 NaCl, 25 $NaHCO_3$, 2.8 KCl, 1.2 KH_2PO_4, 1.2 $MgSO_4$, 1.3 $CaCl_2$, and 5.0 D-glucose. All solutions were equilibrated with a mixture of 95% O_2 and 5% CO_2. In experiments with 7 mM K^+ rather than 4 mM K^+, 3 mM NaCl was replaced by 3 mM KCl to maintain osmolarity. In all experiments, 50 µM *N*-benzyl-*p*-toluene sulphonamide (BTS; Toronto Chemicals) was added to reduce the contractile activity associated with AP firing (Macdonald et al., 2005).

Determination of passive membrane properties and conduction velocities of APs

For measurements of the passive electrical properties and propagating APs in EDL muscle fibers, we used an experimental setup detailed elsewhere (Macdonald et al., 2005; Pedersen et al., 2005). Recordings were low-pass filtered with a cutoff at 10 kHz and sampled at 30 kHz. All sampling used Signal software (Cambridge Electronic Design). Two glass microelectrodes (~20 MΩ) were inserted into the same EDL muscle fiber. To record propagating APs and to obtain their propagation velocities, the motor nerve was stimulated using a suction electrode. The propagation velocity of the resulting AP was determined by dividing the inter-electrode distance by the time between the peak of the AP at the two locations. If the electrodes remained inserted after the AP recordings, the two electrodes were next used for determination of the linear electrical properties of the same fiber. To do this, one electrode was used to inject a square current and sinusoidal currents in the frequency range of 10–800 Hz, while the other electrode recorded the membrane potential at a minimum of three locations along the muscle fiber. Only experiments in which it was possible to obtain both propagating APs and the passive cable properties of the particular fiber were used for analysis.

A grounded shield was introduced between the two electrodes to reduce capacitative coupling between the electrodes. The sinusoidal currents were of sufficiently low frequency to avoid extensive capacitative coupling between electrodes. Nevertheless, negative capacitative feedback circuitry was used to further minimize stray capacitances, and solution levels were kept as low as possible. G_M, r_i, and a (the fiber radius) were determined using square-pulse currents as performed on previous occasions (Hodgkin and Rushton, 1946; Boyd and Martin, 1959; Pedersen et al., 2005). The requisite calculations were based on cable theory derived for the simple cable structure (Fig. 2 A). This is a valid simplification for steady-state or very low frequency-impedance determinations, but, as this paper demonstrates, at higher frequencies the t-system luminal resistance must be taken into consideration. Based on this, only the low frequency capacitance (10 Hz) of the membrane was calculated using the theory developed for the simple cable. This provided a rough estimation of the total membrane capacitance (sarcolemma and t-system) that was used in the model. This membrane capacitance was calculated from the expression:

$$C_m = \frac{-G_m \arctan(\psi)}{2\pi f}, \tag{8}$$

where ψ is the phase of the membrane impedance, $Z_{M,Simple,}$ (see Appendix 1) at 10 Hz.

To obtain values for the frequency-dependent parameters of $Z_{in(f)}, \lambda_{(f),} Z_{M,(f)}$, the injected sinusoidal currents and the resulting sinusoidal changes in membrane potentials were fitted to the following equation:

$$y_{(t)} = y_{(0)} + A\sin(2\pi ft + \theta). \tag{9}$$

This procedure extracted the phase, θ, and the amplitude, A, at each of the three or four locations along the muscle fibers. The term $y_{(0)}$ represents either the resting membrane potential or zero current injection. The phase shift (φ) between the injected current and the membrane voltage response at two locations along the fiber were used to calculate the velocity of the passive current flow along the fibers:

$$Velocity = \frac{2\pi fd}{(\varphi_2 - \varphi_1)}, \tag{10}$$

where $d = x_2 - x_1$ represents the distance between the two locations along the fiber at which the sinusoidal membrane potential responses were measured. This apparent velocity was used for comparison with the circuit models to evaluate which of the models provided the most accurate description of the passive electrical properties of muscle fibers. Any stray capacitance on the

recording electrode would have been the same at the two locations and thereby removed by the subtraction of the phase shifts.

Determinations of G_M in AP-firing muscle fibers

Methods used to measure G_M in fibers firing APs have been described in detail elsewhere (Pedersen et al., 2009a). In brief, two microelectrodes were inserted into a muscle fiber of a BTS-treated muscle. The electrodes were inserted sufficiently close to allow the input resistance ($R_{in} = \Delta V_{DC} / I$) of the fiber to be determined directly when one electrode injects a small square current (I), and the other electrode measures the membrane potential response, ΔV_{DC}. During the experiments, the current injecting electrode alternated between injecting small square currents for determinations of R_{in} and hence G_M, and shorter, larger current pulses used for triggering trains of APs. G_M can be determined from the measured R_{in} between the AP trains using the following relation:

$$G_M = \frac{R_{in,0}^2}{R_{in}^2} G_{M,s}, \tag{11}$$

in which G_M represents the resting membrane conductance in the fiber firing APs, and $G_{M,s}$ represents the resting membrane conductance in quiescent fibers determined under similar experimental conditions using the spatial decay of the voltage response resulting from a square current as described above (Pedersen et al., 2009a; Fig. 1 A). $R_{in,0}$ is the input resistance of the investigated fiber before firing APs, and R_{in} is the input resistance during the AP firing.

RESULTS

Experimental measurement of the cable properties of resting skeletal muscle fibers

This study evaluated the influence of G_M changes in active mammalian muscle fibers on AP initiation, its sarcolemmal conduction, and t-system excitation. It was, however, first necessary to determine an appropriate circuit model for skeletal muscle fibers. This involved experimental measurement of the membrane-impedance properties of rat EDL muscle fibers using a two-microelectrode technique. The observations from these experiments were then compared with the theoretical predictions from three different circuit models to select the most suitable model for further analysis.

Fig. 1 A shows representative recordings of the membrane potential (bottom panel) at three distances along a muscle fiber during the injection of square and sinusoidal currents, the latter with frequencies of 200 and 400 Hz (top panel). The maximum membrane potential deflections in response to these currents were determined either by simply measuring the deflection size (square current) or by fitting a sinusoidal waveform to the recordings (Eq. 9 and Fig. 1 A, red lines in bottom panel) to measure both amplitude and phase of the

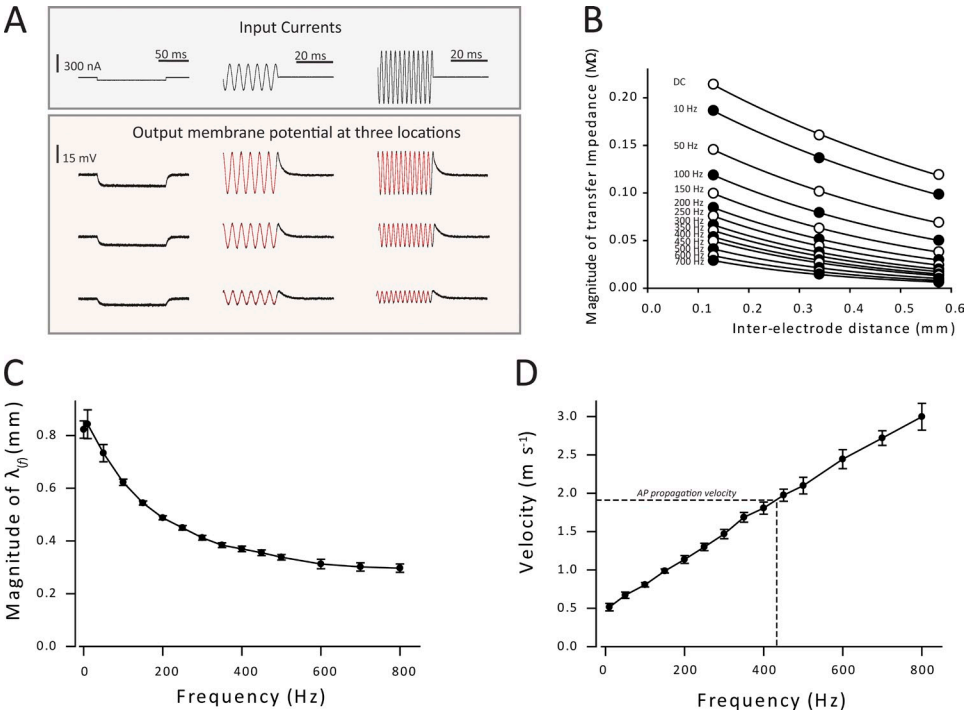

Figure 1. Determination of membrane impedance of EDL muscle fibers. Membrane potential responses to injections of square and sinusoidal currents were determined at three inter-electrode distances. This used an experimental setup with a current-injecting and a membrane potential–recording electrode that was described elsewhere (Pedersen et al., 2005). (A) Examples of injected currents (top panel) and the membrane potential responses observed at the three inter-electrode distances (bottom panel). The red lines in the sinusoidal voltage responses show fits to a sinusoidal waveform. The transfer impedance at each of the three locations along the fiber was then determined from the maximum deflection in membrane potential divided by the amplitude of current injection. (B) Magnitudes of the transfer-impedance moduli for the range of frequencies explored in the fiber also used in A. A simple exponential-decaying function was fitted to the recordings, and from the decay constant, the frequency-dependent length constant could be obtained. (C) The average frequency-dependent length constant for five fibers. In addition to the amplitude of the sinusoidal voltage responses, the fitting also extracted the phase of the voltage responses. This phase data were used to calculate a velocity that reflects the speed by which passive currents flow in a muscle fiber. (D) The velocity by which the different sinusoidal currents propagate as a function of the sinusoidal frequency of the current. Also shown is the AP propagation velocity that was determined in the same fibers that were used for membrane-impedance measurements. Average data are presented as means ± SEM.

membrane potential response. The magnitude of transfer impedance at each inter-electrode distance was then calculated by simply dividing the maximum voltage deflection by the amplitude of the injected current.

The transfer impedance at each frequency was then plotted as a function of inter-electrode distance and fitted to a mono-exponential decaying function (Eq. 4), as shown in Fig. 1 B. The decay constants of these fits were used to determine the magnitude of the frequency-dependent length constants of the fiber. For all inter-electrode distances, the transfer impedance was inversely related to the frequency of the current injections, and the slope of the fits declined with frequency. When this slope was converted to the magnitude of the frequency-dependent length constant (Fig. 1 C), it produced an inverse relation between frequency and this magnitude. Thus, as shown in Fig. 1 C, the average magnitude of the length constant dropped to ~50% of the DC length constant when increasing the frequency from DC to ~400 Hz. Accordingly, it was necessary to use progressively larger currents as the frequency of the sinusoidal currents was elevated. This could potentially bring the membrane voltage at the point of current injection outside the membrane voltage range in which the membrane resistance is constant. However, large currents were only used for the highest frequencies for which the membrane resistance and associated potential nonlinear membrane resistance play a minor role for the membrane impedance, except if APs became excited, in which case recordings were not used. In support of the linear membrane response to the currents, the sinusoidal fits were excellent at all frequencies as would only occur if the membrane response to the sinusoidal currents was indeed linear.

Fits of sinusoidal waveforms to the observed membrane potential responses additionally permitted determination of the velocity by which the passive currents flowed in the fibers using the phase of the waveform at two locations along the fiber (Eq. 10). Because the experimental measurements of membrane impedance included in Fig. 1 had been preceded by measurement of an AP, elicited by stimulating the motor nerve with a suction electrode while the two recording electrodes were inserted at the maximum inter-electrode distance, these experiments allowed comparison of the AP propagation velocity with the velocity of passive current flow. As illustrated in Fig. 1 D, this velocity of passive current flow increased almost linearly with frequency to 800 Hz, and the AP propagation velocity of 1.92 ± 0.11 m s^{-1} was on average matched by the passive propagation velocity of a sinusoidal current of 410 ± 29 Hz ($n = 5$).

Collectively, the observations in Fig. 1 show that higher frequency currents (>400 Hz) only generate small voltage deflections, as reflected by the correspondingly small transfer impedances at such frequencies. In addition, such higher frequency currents decline rapidly with distance, as illustrated by the short length constant at these frequencies. However, the velocity of conduction increased almost linearly with frequency to 800 Hz.

Development of a cable model to reproduce the experimental observations

To determine the cable structure that provided the best representation of these passive electrical properties of a muscle fiber, the observations from Fig. 1 on the magnitude of the frequency-dependent length constant and the velocity of sinusoidal current flow were next compared with theoretical predictions from the three different cable structures. For such comparisons, the models were adjusted for each fiber to match the experimental observations of total DC membrane impedance, fiber diameter, and total membrane capacitance of the particular fiber. Fig. 2 A compares the experimental observations with the simple cable structure (left) that does not include a t-system luminal resistance. For this cable structure, the predicted length constant was much smaller than the experimentally recorded value (Fig. 2 A, middle), and the predicted velocity of sinusoidal current flow deviated clearly from the experimental recordings (Fig. 2 A, right).

Inclusion of a t-system luminal resistance in the cable structures gave a much better agreement between experiment and theory. This resistance was mimicked using two different approaches. In the lumped cable structure (Fig. 2 B, left), the luminal resistance was a lumped resistance placed in series with the circuit components that mimic the t-system membrane. Such a circuit represents a t-system where the dominant resistance of its lumen would be located exclusively at the junction between the sarcolemma and the t-system membranes, that is, at the opening of the t-tubules. When this access resistance, R_A, was set at either 10 or 20% of the DC impedance, the predicted values of the length constant agreed reasonably well with the experimental observations. However, the agreement of theory and experiment was less convincing for the velocity of passive current flow, for which the predicted velocities of intermediate frequencies (150–700 Hz) were too low with R_A at 10% and too high with R_A at 20% of DC impedance.

In the other cable structure that included a t-system luminal resistance, the distributed cable structure, the t-system was modeled as 20 concentric shells with luminal resistances between shells (Fig. 2 C, left). This represents a t-system where the luminal resistance simply results from the small diameter of the t-tubules and is therefore distributed throughout the t-system, rather than being located solely at the junction between the sarcolemma and the t-system membranes. These simulations were conducted for a range of t-system luminal resistivities for each fiber and compared with the experimental results. The close agreement between the

shapes of the experimental and theoretical curves for the magnitude of the frequency-dependent length constant and the velocity of the passive current flow allowed quantification of the t-system resistivity. Thus, both the length constant and propagation velocity of sinusoidal currents closely agreed with the experimental observations when the resistivity of the t-system lumen on average was set at 154 ± 27 Ω cm and the diameter of the t-tubules was 120 nm as determined histologically for rat EDL by Cullen et al. (1984). These analyses strongly indicated that the t-system lumen exerts a significant resistance to current flow, even for frequencies only slightly above DC. This further implies that it is necessary to include this resistance when modeling the electrical properties of the passive muscle fiber membrane.

The influence of the t-system luminal resistance on the matching of the passive electrical membrane properties and AP frequency content to the AP propagation velocity

During AP propagation, the local circuit currents responsible for both propagating the sarcolemmal AP and exciting the t-system AP are generated by the intracellular

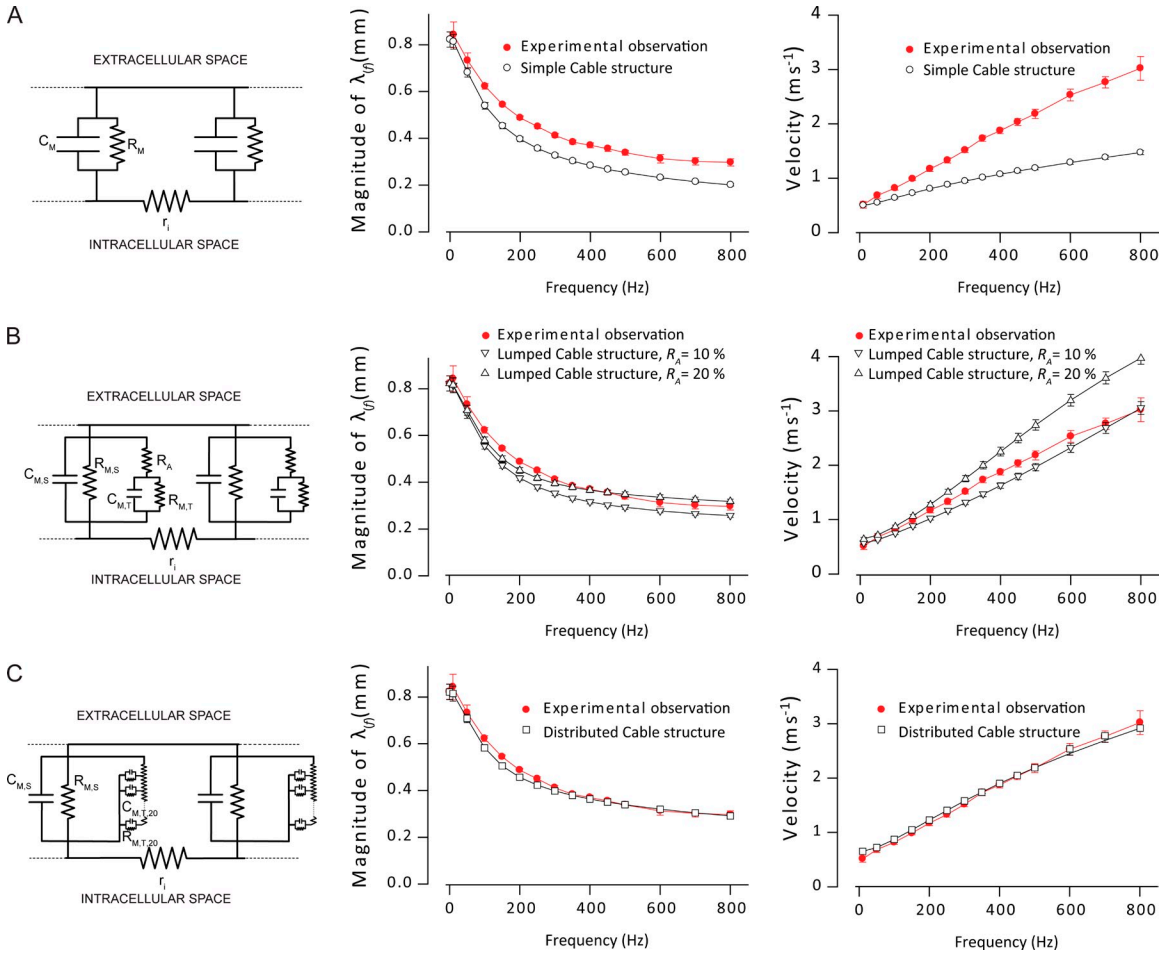

Figure 2. Effect of t-system luminal resistances on passive electrical properties of rat EDL muscle fibers. Experimentally determined frequency-dependent length constants (middle panels) and the propagation velocities of sinusoidal currents (right panels) were compared with theoretical predictions from three cable structures (left panels). These models either omitted (A) or included the t-system luminal resistance (B and C). The dotted lines in the circuit representations of the different cable structures indicate that the structures are of infinite length. When experimental observations from a fiber were compared with theoretical predictions from a cable structure, the model dimensions were initially adjusted to match the experimentally determined diameter, DC impedance, and the total capacitance of the particular fiber. The SEM bars for the model output, therefore, indicate the variation in the length constant and velocity that resulted from these adjustments. (A) Comparison of the experimentally determined length constant (middle) and propagation velocity of sinusoidal currents (right) with theoretical predictions from the simple cable structure, which did not include a t-system luminal resistance. (B) A similar comparison of experimental data and theoretical predictions from the lumped cable structure when its lumped t-system lumen resistance, the access resistance R_A, was set to either 10 or 20% of the DC impedance of the fiber. (C) In the distributed cable structure, the t-system was divided into 20 shells, and the t-system luminal resistance was accordingly distributed in between these shells. The experimental data has been compared with theoretical predictions when the t-system luminal resistance was varied by changing the resistivity of the t-tubular volume. Average data are shown as means ± SEM.

voltage difference between source and sink membrane regions. Clearly, these circuit currents must propagate at least as fast as the propagating AP. Building on this notion, we further investigated the influence of a t-system luminal resistance by comparing experimental observations of the propagation velocities of both sinusoidal currents and APs with the frequency content of recorded APs. These experimental observations were then related to the different circuit models.

Fig. 3 A shows voltage changes at two locations during a typical experimentally recorded AP in a rat EDL muscle fiber. Such recordings gave a mean AP propagation velocity of 1.92 ± 0.11 m s^{-1} (n = 5). The frequency content of such APs was extracted by Fourier transformation, and the average power spectrum of the APs is shown in Fig. 3 B. The detailed features at the lower frequencies were clarified by presenting the frequency content along a logarithmic rather than along a linear scale as can be done using the Fourier transformation method described by Huang (1983). The power spectra showed that the majority of the frequencies in the AP were concentrated between DC and 1 kHz, and the AP was effectively band-limited at 2 kHz. Thus, the median frequency of the APs was 396 ± 15 Hz (Fig. 3 C), and the spectrum had declined to around 10% of its DC value at 1,113 ± 147 Hz. Interestingly, the median frequency of the AP waveform roughly corresponds to the experimental determinations of the frequency that a sinusoidal current must have to at least conduct with a passive velocity similar to that of the experimentally recorded AP (see Fig. 1 D). We will term the frequency of a sine wave that conducts passively with the same velocity as an AP the "equivalent frequency" of that AP.

Fig. 3 D shows the equivalent frequency for each of the three cable models. Including a luminal resistance reduced the equivalent frequency by around 70% when compared with the simple cable. Furthermore, these equivalent frequencies in both the lumped and distributed cable structures closely mimic the experimentally recorded velocities of sinusoidal currents (Fig. 2) as well as the frequency content of APs (Fig. 3 B). Thus, a t-system luminal resistance is required for the passive membrane properties and the frequency content of propagating APs to match the AP propagation velocity.

The physiological significance of t-system luminal resistance

Having quantified the t-system luminal resistance in a mammalian skeletal muscle fiber, we next explored aspects of the functional significance of such resistances for sarcolemmal AP initiation and propagation and t-system excitation. A linear systems approach involved the convolution of transfer functions describing the linear cable structures (Fig. 2, left panels, and Eqs. 4 and 5) with either a square current pulse of 1-ms duration to mimic AP initiation by an electrotonic endplate current,

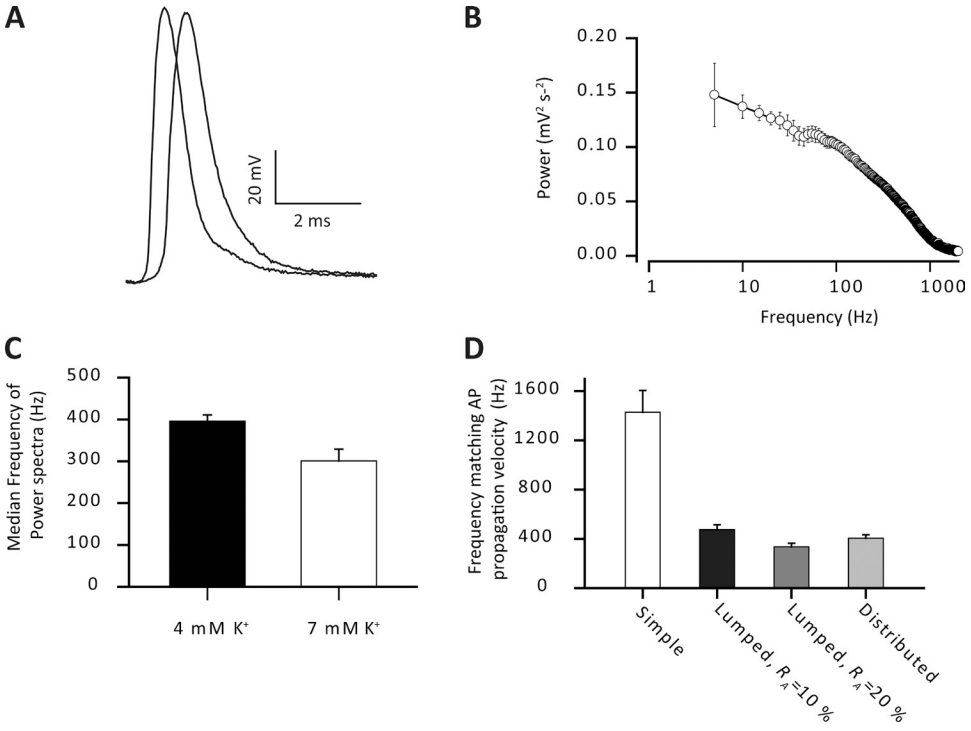

Figure 3. Fourier transform of propagating APs. An AP was elicited using a suction electrode stimulating the motor nerve to a muscle fiber impaled with two electrodes inserted at the maximum inter-electrode distance before the determinations of the fiber impedance properties shown in Fig. 1. (A) Typical experimental recordings of an AP at two locations along the same muscle fiber. (B) Average power spectrum of propagating APs. Note the logarithmic abscissa. (C) From such power spectra the median frequency was determined. Such an analysis was also performed under conditions of moderately elevated extracellular K^+ (7 rather than 4 mM) to mimic extracellular conditions in active muscle. Recordings similar to those in A were used to determine the AP propagation velocity of 1.92 ± 0.11 m s^{-1}. Such AP propagation velocity must naturally be conveyed by elements of the circuit currents in front of the AP that propagate with at least the same velocity as the AP. To determine the relevant frequency components of these circuit currents for AP propagation, the velocity of sinusoidal currents that reached the AP velocity, the equivalent frequency, was experimentally determined to be 410 ± 29 Hz in Fig. 1. (D) The equivalent frequencies in the three cable structures. Average data are shown as means with SEM.

or with an experimental recording of a propagated AP to mimic the circuit currents during AP propagation. Such circuit currents have the dual role of both propagating the sarcolemma AP and exciting the t-system. The outcome of this analysis is illustrated in Fig. 4. Starting from the left-hand side, the first three panels of Fig. 4 A show the computed voltage profiles over distance in the three cable structures depicted in Fig. 2 during the application of a 1-ms square current pulse. Each line represents spatial voltage profiles that are separated in time by 100 µs, starting 100 µs after the current was applied. The panel to the far right in Fig. 4 A shows an overlay of these voltage profiles from the three cable structures. This shows that inclusion of a luminal resistance in the t-system, which can either be lumped or distributed, gives rise to a more rapid rise in the voltage profiles. Thus, the area under the voltage profile curves after 100 µs was approximately two and a half times larger in the cable structures with the luminal resistance as compared with the voltage profile in the simple cable where this resistance had been omitted. Similarly, inclusion of the t-system luminal resistance led to a substantially

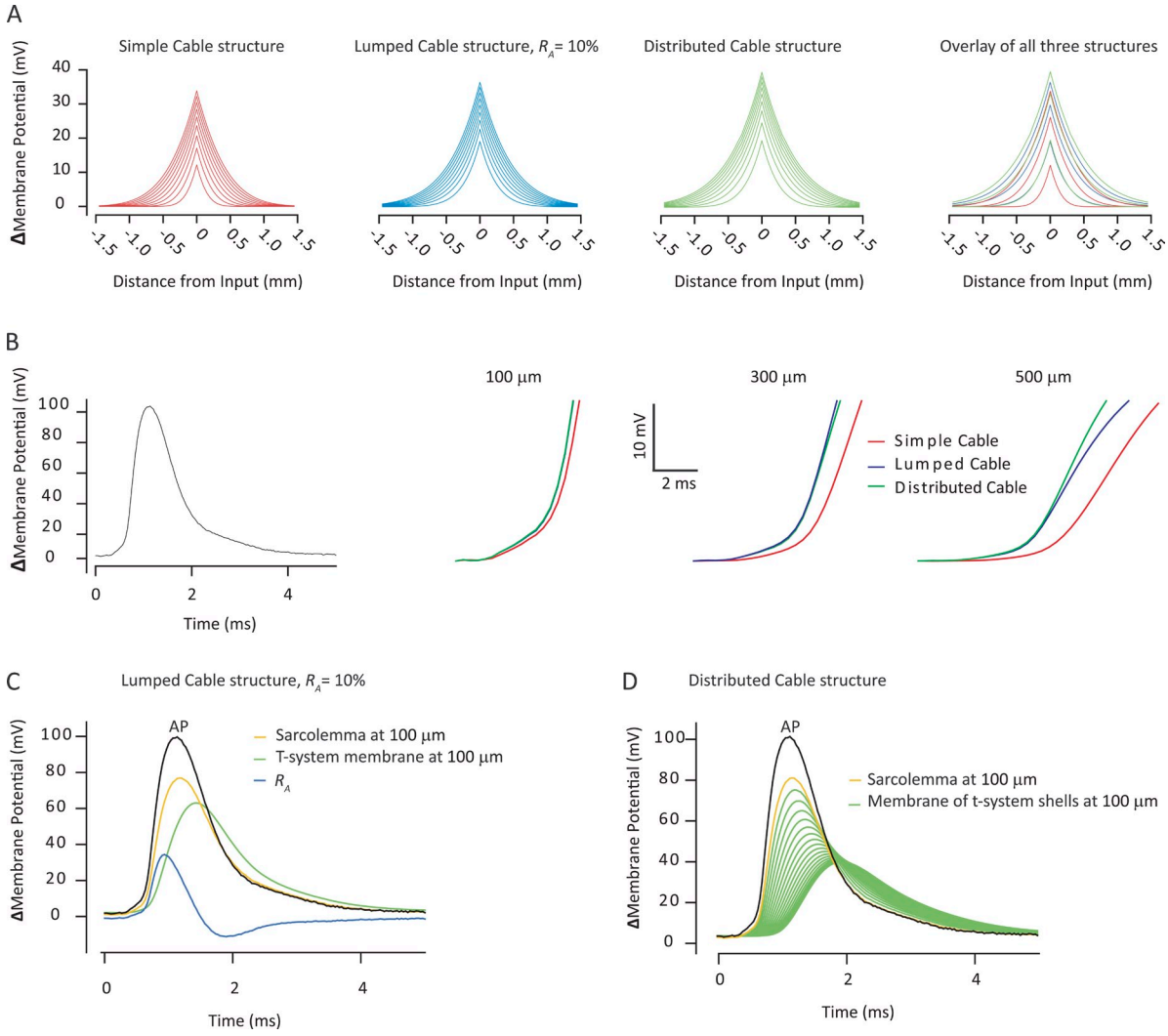

Figure 4. The presence of a t-system luminal resistance enhances the voltage response to a short duration current similar to the end-plate current and increases the velocity of passive current flow in front of a propagating AP. (A) Shows the spatial voltage profiles in both directions away from the point of application of a 1-ms square current pulse, calculated from a convolution of the transfer functions that describe the cable structures in Fig. 2 (left panels) with a 1-ms square current pulse. This was used to mimic the subthreshold events in sarcolemmal AP initiation. The successive lines represent the profile in steps of 100 µs after the initiation of current application. In the far right panel, the voltage profiles at 100, 500, and 900 µs in the three cable structures have been overlaid for comparison. (B) Similarly computed passive sarcolemmal voltage responses 100, 300, and 500 µm in front of a propagating AP (left). These voltage responses have been truncated at 25 mV to depict the initial rise of the passive response in the sink membrane region in front of the propagating AP. (C) Computed passive voltage responses of the sarcolemma, the access resistance, and the t-system membrane to the application of a recorded AP in the lumped cable structure. (D) The passive voltage responses in the distributed cable across the sarcolemma and the t-system membrane shells when a propagating AP is used as input function. Note that in C and D, the passive voltage responses were not truncated at 25 mV and thus extend into a membrane potential that would lead to activation of voltage-gated Na^+ channels.

larger and broader voltage profile at the end of the current application. These simulations suggest that for short duration current flow, like the endplate current, the t-system luminal resistance enhances the peaks of electrotonic potentials and broadens their voltage profile away from the site of stimulation.

To assess the functional role of the t-system luminal resistance for sarcolemma AP propagation, an experimentally recorded AP (Fig. 4 B, left) was convolved with the three cable structures, and the resulting passive voltage responses were determined at three locations in front of the AP (Fig. 4 B, three right panels). Because linear analysis is limited to exploring membrane phenomena in the range of membrane potentials in which the membrane behaves like a linear system, this analysis was only concerned with the initial upstroke of the voltage responses, the foot of the AP, which reflect the passive charging of the membrane sink region during AP propagation. This, analysis clearly showed that the inclusion of a luminal resistance in the t-system leads to a faster rise of the passive charging in the sink membrane region during AP propagation. The physiological significance of this finding is that the t-system luminal resistance would enhance the velocity by which the circuit currents in front of the AP are flowing and should thereby enhance the velocity with which an AP propagates.

The final analysis of the physiological role of the t-system luminal resistance evaluated its effect on t-system excitation. Because omitting this resistance in the simple cable structure implies that the sarcolemma and t-system APs should occur simultaneously and be of identical shape, this analysis was restricted to the lumped and the distributed cable structures. T-system excitation occurs via currents that charge the t-system membrane but also pass through the t-system luminal resistance. The voltage from the intracellular space to the interstitium is then the sum of the voltage responses across the t-system membrane and the t-system luminal resistance. However, only the former voltage response acts to excite the membranes of the t-system. Fig. 4 C illustrates the results of computations of the voltage responses that would be expected in the lumped cable structure in response to the application of an experimentally recorded AP (Fig. 4 C, black line). Results were evaluated at 100 µm from the point of input application, and the yellow line illustrates the voltage across the sarcolemma 100 µm in front of the AP application. The green line shows the t-system membrane response, and the blue line shows the voltage change across R_A. Note that the voltage response of the t-system membrane is entirely passive; therefore, it only correctly predicts the voltage response in the subthreshold voltage range. The reason for the inclusion of the entire voltage response of the t-system membrane is that it was required to illustrate the voltage division between R_A and the membrane of the t-system and for the Fourier transform used below. The conclusions obtained from the present study are tested in our companion study (Fraser et al., 2011) under conditions where the t-system membrane contains the nonlinear properties necessary to excite APs.

This investigation shows that during the early parts of the surface membrane depolarization, the voltage response across the t-system membrane and R_A resided entirely across R_A. In the later stages of the sarcolemma membrane voltage change, the voltage response across R_A decayed, whereas the voltage across the t-system membrane was building up. This suggested that most of the voltage response from the intracellular space to the interstitium resided across R_A for high-frequency components of the passive charging of the t-system, whereas lower frequency components were responsible for charging the t-system membrane. To explore this in detail, the voltage responses in Fig. 4 C were Fourier transformed, and the median frequencies of their spectra were evaluated using the approaches described for Fig. 3. This analysis showed that at 100 µm in front of the AP application, the power spectrum of the passive t-system membrane response had a median frequency of 213 Hz, whereas the median frequency of the voltage response across R_A was 546 Hz. This directly shows that the low frequency components of the local circuit currents are important for exciting the t-system AP.

Convolution of the recorded AP with the transfer function of the distributed cable structures and extraction of the voltage responses across each of the t-system membrane shells (Appendix 1) yielded results similar to those shown from the lumped cable. Fig. 4 D similarly shows the recorded AP that was used as input function (black line), the sarcolemma passive response 100 µm from the point of its application (yellow line), and the voltage drops across the t-system membrane shells at this location (green lines). The magnitudes of the passive responses of the different t-system shells were inversely related to the depth of the t-system, such that the deeper part of the t-system displayed progressively smaller and more delayed voltage responses. Such a display demonstrated that the t-system, particularly the outer shells, was capable of substantial passive excursions in voltage in response to surface AP activity. The median frequency of the voltage response across the membrane of the outer t-system shell was 273 Hz, whereas the median frequency was reduced to 152 Hz for the innermost shell.

Dynamics of G_M during AP firing in rat EDL muscle fibers

Collectively, the analyses in Fig. 4 (B–D) show that during AP propagation, the high frequency component of the local circuit currents is important for surface AP propagation, whereas the low frequency components are important for exciting the t-system AP. Because G_M predominantly affects low frequency membrane impedance, this suggests that the changes in G_M recently reported

during AP firing in active muscle fibers (Pedersen et al., 2009a,b) are likely to have contrasting effects on sink regions in the sarcolemma and t-system during excitation and AP propagation. To investigate this, the present study first confirmed the findings of a highly dynamic G_M in AP-firing fibers of rat. For such experiments, two microelectrodes were inserted in the same fiber at close proximity. One electrode was used to inject a current protocol that consisted of a series of small square current pulses that were used to measure G_M (Eq. 11), followed by a train of larger and shorter depolarizing pulses to trigger APs. This current injection protocol (cycle) was repeated until 4,998 AP-firing pulses had been injected. The second electrode was used to measure the membrane potential throughout the experiment.

Fig. 5 (A–C) shows representative recordings of membrane potential from a fiber during the first, the 29th, and the 81st current injection cycle. The underlined voltage responses to the small diagnostic square current pulses in Fig. 5 (A–C) that were used for G_M determinations in between the AP trains have been enlarged in Fig. 5 (D–F). G_M was assessed from the size of the steady-state voltage deflection of these pulses (ΔV_{DC}). This avoided interference from the membrane capacitance in the measurement of G_M. An increased ΔV suggests ion channel inhibition and a consequent fall in G_M. Conversely, a reduced ΔV_{DC} indicates ion channel opening and an increase in G_M. Confirming the previous observations, ΔV_{DC} initially increased during AP firing (compare Fig. 5, A with B, and D with E), whereas with

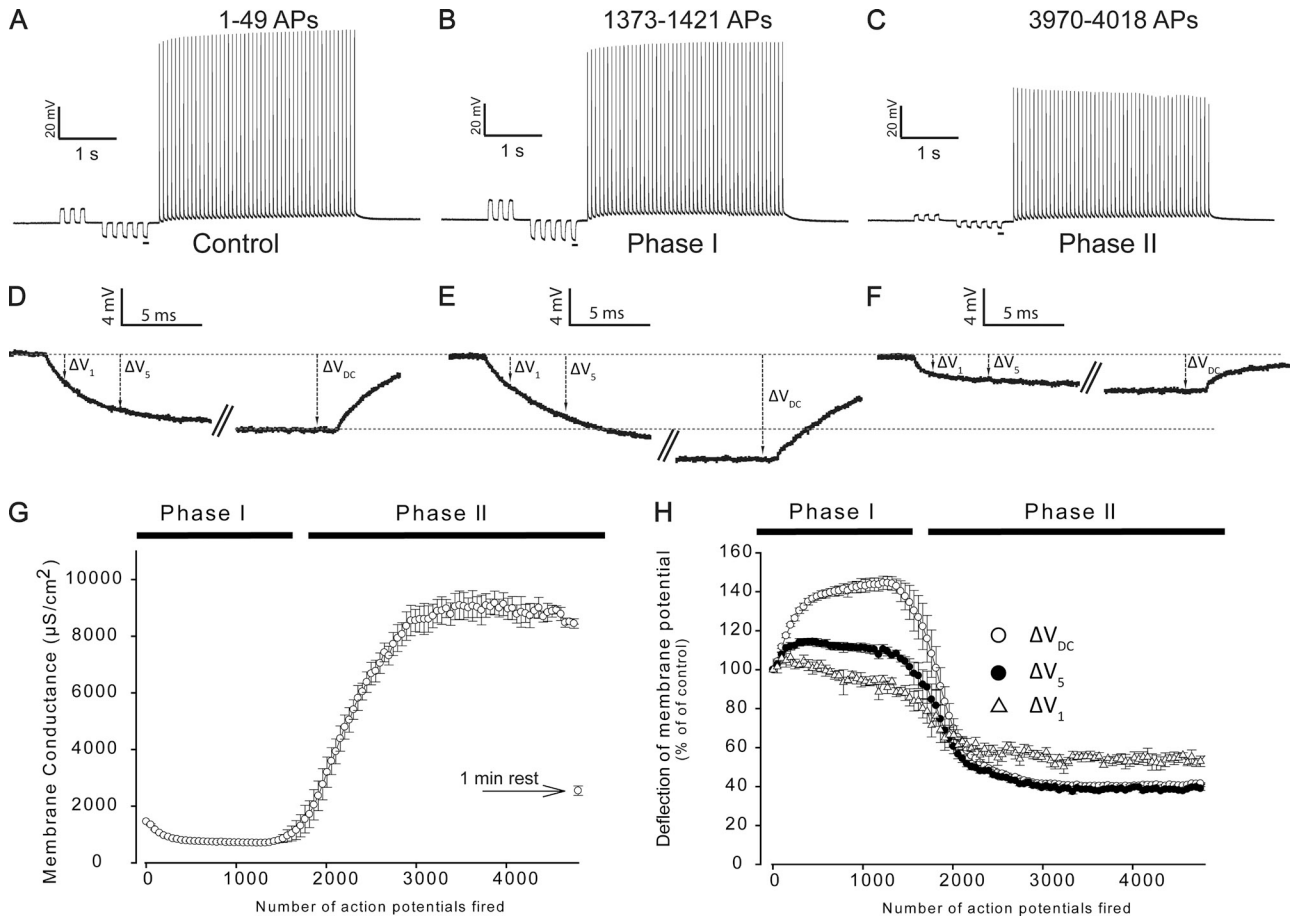

Figure 5. Biphasic changes in G_M during intermittent AP firing in EDL muscle fibers. Two microelectrodes impaled the same fiber of a BTS-treated muscle. One electrode was used to inject a current protocol, and the other electrode was used to measure the membrane potential. Each stimulus cycle in the experimental protocol began with a series of small square current pulses, whose resulting voltage responses could be used to obtain G_M (Eq. 11). This was followed by a train of 49 larger AP-triggering pulses, after which the stimulus cycle was repeated until a total of 4,998 AP-triggering pulses had been delivered. Next, a 1-min rest period was given before a final delivery of the stimulus cycle to assess fiber recovery. (A–C) The first, 29th, and 81st of such AP trains. (D–F) Enlargements of the underlined membrane potential responses to the small current injections in the recordings of AP trains depicted above. The magnitudes of these membrane potential responses to the small currents were determined after ~75 ms of current injection when a stable deflection was obtained (ΔV_{DC}) and used for G_M determination. (G) The average G_M over such experiments ($n = 5$). The deflections of membrane potential in response to the small current injections in between the AP trains were also determined after 1 and 5 ms of current injection (ΔV_1 and ΔV_5, respectively). (H) Average observations of ΔV_1, ΔV_5, and ΔV_{DC} in the experiments. Average data are presented as means with SEM.

prolonged AP firing, ΔV_{DC} dropped well below the initial control level (compare Fig. 5, A with C, and D with F). These changes in ΔV_{DC} were then used to calculate G_M (Eq. 11) throughout the experiment. Thus, Fig. 5 G shows that at the onset of AP firing, G_M dropped to ~40% of its level before AP firing (Phase I), whereas with prolonged AP firing, G_M suddenly rose to >500% of the starting level (Phase II). Finally, if the stimulation was ceased for 1 min after 4,998 AP trigger pulses, G_M recovered completely.

Biologically relevant currents, such as the electrotonic currents after endplate excitation and the circuit currents during AP propagation, are of much shorter durations than the currents that were used for G_M determination. Thus, to evaluate the effect of G_M dynamics on such shorter timescales, the membrane potential deflections in between the AP trains were also determined after 1- and 5-ms durations (ΔV_1 and ΔV_5, respectively). Fig. 5 H shows that the deflections were largest for ΔV_{DC}, of intermediate magnitude for ΔV_5, and smallest for ΔV_1 during both Phase I and Phase II. Although this suggests an inverse relation between the effect of G_M changes and the duration of the membrane current, the effect of G_M changes in active muscle was apparent for even the shortest currents during Phase II.

The physiological significance of G_M dynamics for AP initiation, AP propagation on the sarcolemma, and t-system excitation

The functional significance of the observed changes in G_M in active muscle fibers for AP initiation, as occurs during neuromuscular transmission, sarcolemma AP propagation, and t-system excitation was next explored using the distributed cable model. The analysis assumed that such G_M changes occurred uniformly in both sarcolemmal and the t-system membranes, although it has not yet been possible to determine experimentally in which subcellular membrane region (sarcolemma vs. t-system) that the regulation of ion channels that underlie the G_M changes actually occurs.

Fig. 6 A shows electrotonic voltage profiles produced by the application of 1-ms square current pulse similar to the endplate current during neuromuscular transmission. The decrease in G_M during Phase I only marginally enhanced these electrotonic responses when compared with the corresponding control traces. Thus, at the end of the current application, the area under the voltage profile during Phase I was only 5% larger than that observed during control conditions. In contrast, increases in G_M after sustained AP firing in Phase II (Fig. 5) markedly reduced the area below the electronic potentials by ~50%. Thus, although the observed reduction in G_M at the onset of AP firing only marginally enhances the generation of electrotonic potentials, its subsequent increase after prolonged firing could markedly compromise AP initiation at the neuromuscular junction.

Fig. 6 B examines how G_M changes in the sink membrane could affect sarcolemmal AP conduction velocity. As in Fig. 4 B, a recorded AP waveform (Fig. 6 B, left) was convolved with the distributed cable structure with G_M set to values reminiscent of control, Phase I, and Phase II. Neither reductions in G_M during Phase I nor its elevations during Phase II significantly affected the passive voltage responses in advance of the AP waveform, the foot of the AP. This suggests that the G_M changes during AP firing (Fig. 5) would not markedly interfere with sarcolemmal AP propagation, provided that the ionic currents underlying the AP are otherwise unaffected.

In contrast, analysis of the voltage responses in the t-system membrane shells 100 µm in front of the AP waveform shows that the G_M changes significantly influenced the electrical responses of the t-system to a sarcolemmal AP. Fig. 6 C shows the voltages across the sarcolemma (yellow lines) and the t-system membrane shells (green lines) under control conditions (left) and through the G_M changes during Phase I (middle) and Phase II (right). Note that again, the voltage responses across the t-system membranes are entirely passive. The reasons that these responses were not truncated at 25-mV voltage deflection as appropriate for a linear membrane and as done in Fig. 6 B are twofold: first, it was necessary to use the entire waveform for the Fourier analysis of the voltage responses down through the t-system (see above); and, second, it was interesting to note that even in the innermost t-system shell, the passive responses were so large that they should activate voltage-gated Na^+ channels. This suggests that under normal conditions and during Phase I, the sarcolemma AP activates voltage-gated Na^+ channels and excites the t-system more or less uniformly, thus making propagation of the t-system AP minimal under control conditions. The decrease in G_M occurring during Phase I resulted in larger and broader voltage responses across the t-system membrane shells compared with those obtained under control conditions, particularly in the deeper parts of the t-system. Thus, the area below the voltage response of the deepest shell of t-system membrane was ~25% larger than in the corresponding shell under control conditions. Correspondingly, the increased G_M during Phase II markedly reduced both the amplitudes and durations of the voltage changes across the t-system membrane shells. The voltage response of the deepest t-system membrane shell dropped to ~15% of the response in the corresponding membrane shell under control conditions. Thus, in contrast to the situation in sarcolemmal membrane, the existence of a low-pass–filtering action of the tubular luminal resistance makes t-system excitation highly dependent on G_M and suggests that excitation–contraction coupling can be regulated in active muscle by dynamic changes in G_M.

To mimic conditions in working muscle where extracellular K^+ is increased (Hník et al., 1976; Nielsen et al., 2003),

further simulation studies went on to explore for graded effects of elevations in extracellular [K^+], also known to take place during sustained AP firing. Fig. 7 illustrates the results of such an exploration that used AP waveforms recorded at a higher (7 instead of 4 mM) extracellular [K^+], which had lower amplitude and a power spectrum with a reduced median frequency (Fig. 3 C). It assumed that the increased [K^+] to 7 mM roughly doubled G_M even under control conditions as can be predicted from constant field theory (Eq. 6.0 in the appendix of Hodgkin and Katz, 1949). Such dependence of G_M on extracellular [K^+] has been experimentally verified in mammalian muscle (Kwieciński et al., 1984; Pedersen et al., 2005). The increased [K^+] accentuated the effect of increasing the electrotonic potentials with Phase I and, more markedly, further reduced the electrotonic potentials during Phase II (Fig. 7 A). Surface propagation of the AP would largely remain spared as the passive response in front of the AP was largely unaffected by the G_M changes except during Phase II for the largest distance (Fig. 7 B). However, although the increase in tubular excitation during Phase I was only slightly larger at moderately

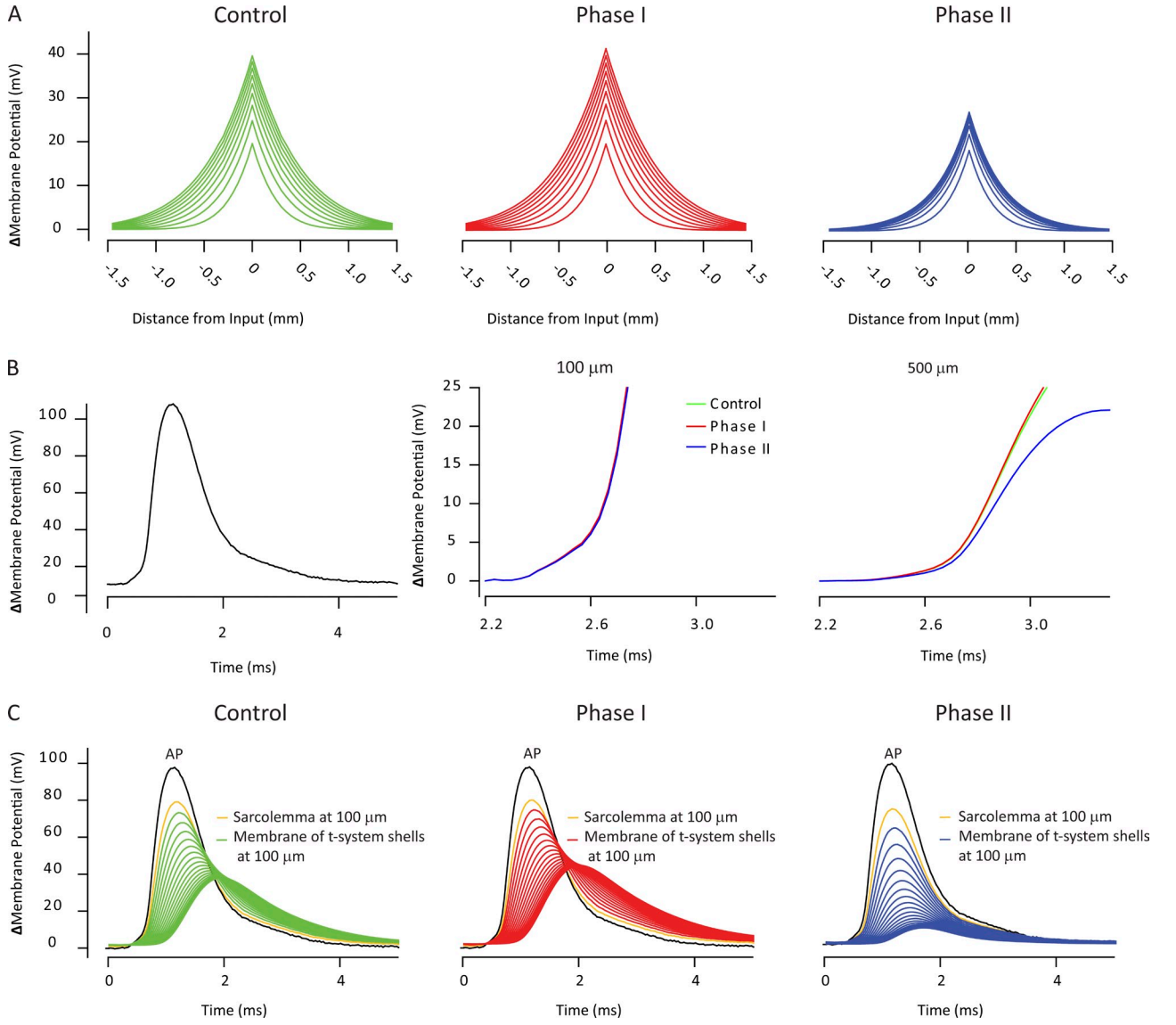

Figure 6. Alterations in G_M taking place during sustained activity in muscle fibers affect sarcolemmal AP initiation and t-system excitation in preference to sarcolemma AP propagation. In all simulations, the distributed cable structure was used. (A) The spatial voltage profiles in steps of 100 µs of simulated electrotonic potentials similar to endplate potentials when G_M in the models was modified to mimic control conditions (left), conditions during Phase I (middle), and conditions during Phase II (right). (B) A recorded AP waveform (black line, left) was used as the input function in the convolution to evaluate the passive voltage response in front of the AP. Colored lines show the initial (to 25 mV) passive sarcolemmal responses 100 and 500 µm in front of the AP. (C) The voltage responses of the sarcolemma (yellow line) 100 µm in front of the AP waveform (black line), and the voltage responses in the 20 t-system shells at this position during control (green), Phase I (red), and Phase II (blue).

elevated extracellular K^+ when compared with conditions of normal extracellular K^+, the excitation was markedly more depressed in Phase II at elevated K^+.

Further increases in extracellular [K^+] led to more clear effects of the G_M reduction during Phase I. Thus, Fig. 8 demonstrates that when simulating extracellular [K^+] of 12 mM, the reduction in G_M during Phase I produced larger effects on the electrotonic potentials (Fig. 8 A) and t-system excitation (Fig. 8 C) when compared with control and conditions with moderately elevated K^+. Thus, the area of the membrane voltage response in the deepest t-system shell was more than doubled during Phase I. In contrast, even at the largest elevation in extracellular [K^+], the surface conduction would be only moderately affected by the G_M changes (Fig. 8 B). However, during Phase II, the large increase in G_M produced

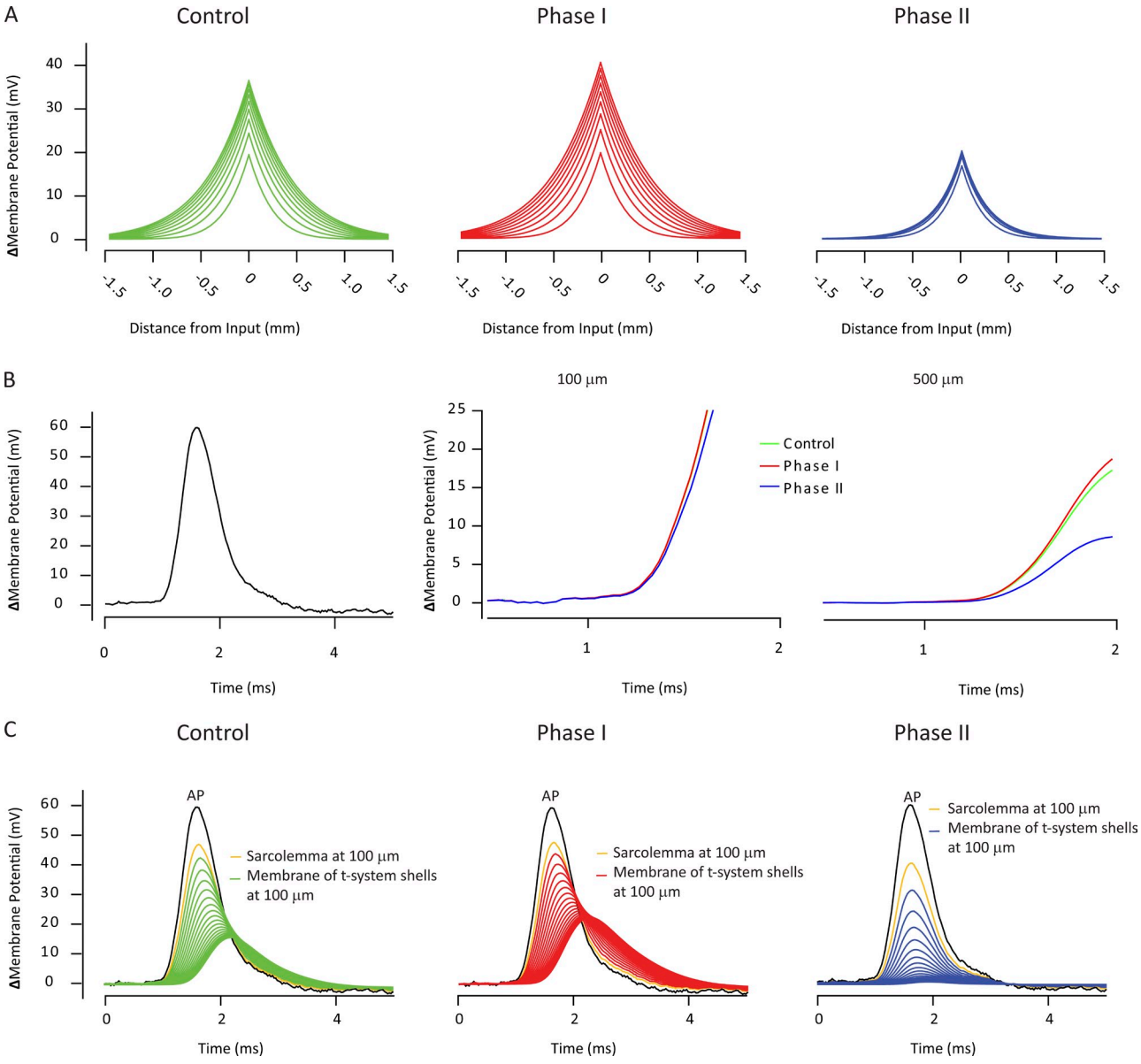

Figure 7. The impact of alterations in G_M in AP-firing muscle fibers on AP initiation, sarcolemma AP propagation, and t-system excitation are all more pronounced when membrane excitability is depressed and muscles are experiencing elevated extracellular K^+. The simulations were designed to mimic additional G_M changes resulting from a moderate elevation in extracellular [K^+] to 7 mM. (A) The spatial voltage profile in steps of 100 µs of simulated electrotonic potentials similar to endplate potentials when G_M in the models was adopted to mimic control conditions (left), conditions during Phase I (middle), and conditions during Phase II (right). (B) Passive sarcolemmal voltage responses to a recorded AP (left) when G_M was set to mimic control conditions, Phase I, and Phase II. Colored lines show the initial (to 25 mV) passive sarcolemmal responses 100 and 500 µm in front of the AP. (C) The voltage responses of the sarcolemma (yellow line) 100 µm in front of the AP waveform (black line), and the voltage responses in the 20 t-system shells at this position during control (green), Phase I (red), and Phase II (blue).

a marked decline in both amplitude and duration of the passive voltage changes across the t-system membrane shells (Fig. 8 C). The voltage response of the deepest t-system membrane shell dropped to ∼1% of the response in the corresponding membrane shell under control conditions at 12 mM K^+. These observations illustrate that in contrast to the situation in sarcolemma membrane, t-system excitation is highly dependent on G_M because of the low-pass–filtering action of the tubular luminal resistance. This suggests that excitation–contraction coupling is regulated in active muscle by dynamic changes in G_M.

DISCUSSION

This study analyzed the role of the regulation of the resting sarcolemmal and t-system membrane conductances that occur in active muscle activity upon AP initiation and propagation over the sarcolemma and upon excitation of the t-system in mammalian skeletal muscle. It follows from recent studies (Pedersen et al., 2009a,b) that demonstrated a PKC-dependent inhibition of ClC-1 channels reducing the total membrane conductance, G_M, to ∼40% of its resting level with the onset of AP firing in rat EDL and soleus muscle fibers. Furthermore, with sustained AP firing (>1,800 APs) G_M abruptly and reversibly increased to ∼500% of its initial value but only in EDL fibers. This increase in G_M reflects coordinated opening of both K_{ATP} and ClC-1 channels (Pedersen et al., 2009a).

This study confirmed these biphasic changes in G_M during AP firing in fast-twitch EDL fibers with an initial decrease (Phase I) followed by a subsequent large increase

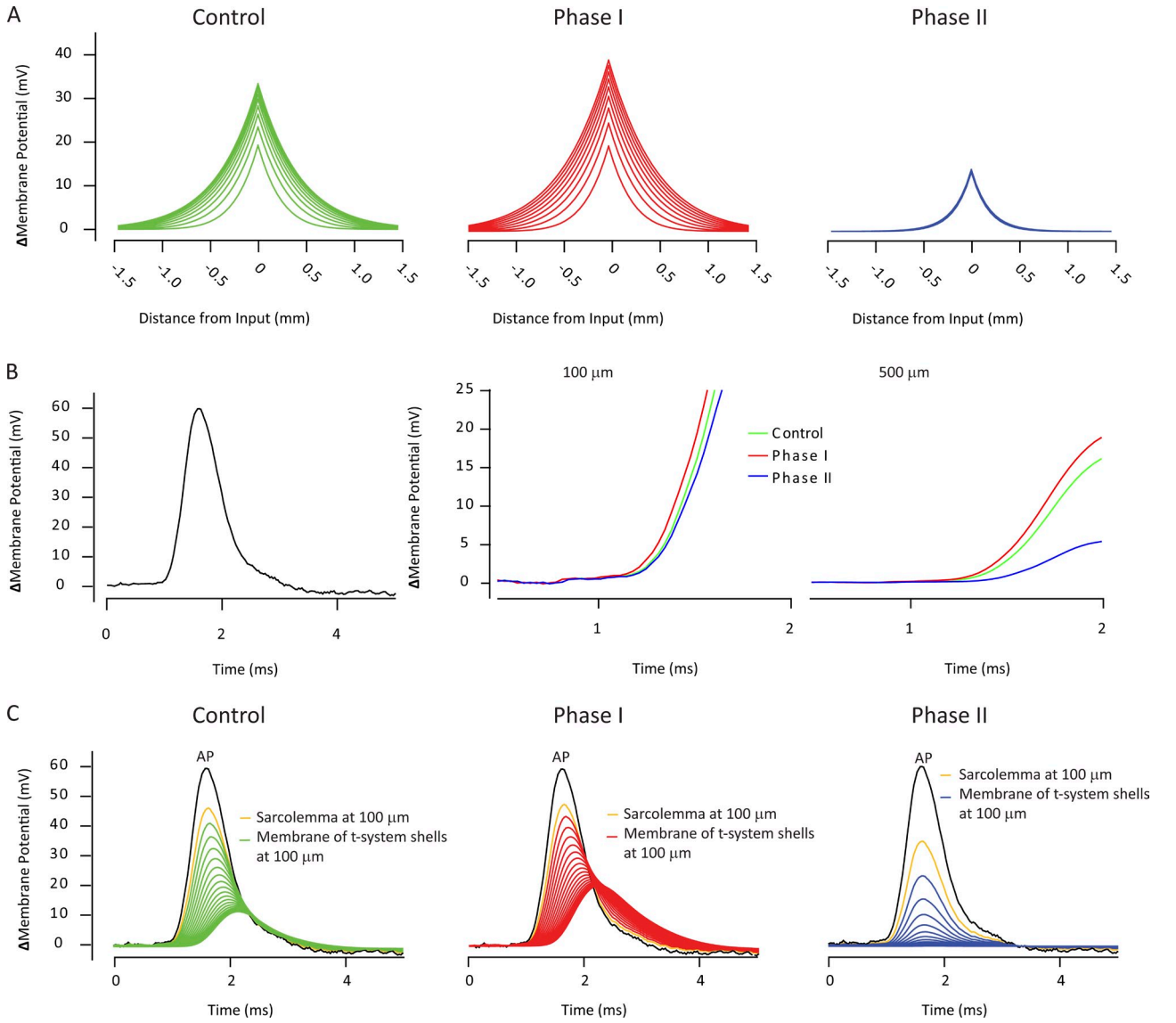

Figure 8. Alterations in G_M during AP firing strongly affect neuromuscular transmission and t-system excitation at high extracellular K^+. In all simulations, the distributed cable structure was used and conditions were designed to mimic conditions with extracellular K^+ of 12 mM. (A–C) As in Fig. 7.

(Phase II), and demonstrated that these changes were evident even during the early (1- and 5-ms) components of the membrane potential deflections resulting from the injections of square current pulses, with the most marked effects during Phase II. This suggested that G_M dynamics during AP trains can influence excitation and conduction properties during a time window that would be relevant for AP initiation, AP propagation, and t-system excitation.

Classical studies suggest that G_M has little influence on membrane excitability in nerve fibers (Hodgkin and Huxley, 1952; Noble, 1972). Yet, several experimental studies have shown that skeletal muscle excitability is inversely related to G_M (see Introduction). The present study aimed to reconcile these findings by exploring the influence of the t-system upon the electrophysiological properties of muscle fibers and hence upon the relationship between G_M and excitability.

Skeletal muscle fibers differ from nerve fibers in that they contain extensive invaginating t-systems (Peachey, 1965; Dulhunty, 1984; Dulhunty et al., 1984; Stephenson, 2006) accounting for ∼80% of their total membrane area. The narrow diameter of the t-tubules (∼120 nm) suggests significant resistance to current flow during AP excitation and propagation. Indeed, this has previously been observed and modeled in amphibian muscle by an access resistance in series with either a single capacitive element (Falk and Fatt, 1964), or more anatomically realistic lattice geometries (Adrian et al., 1969a; Eisenberg, 1983). Such tubular representations explained several electrophysiological properties unique to muscle fibers. These included the after-potentials of experimentally recorded APs (Adrian and Peachey, 1973) as well as the separation of surface and tubular AP components after temperature change (Padmanabhan and Huang, 1990). In addition, Sheikh et al. (2001) had reported similar sarcolemmal conduction velocities both before and after tubular detachment produced by osmotic shock, consistent with a situation in which the existence of tubular luminal resistances minimized the effective tubular capacitative load on sarcolemmal AP conduction (Sheikh et al., 2001).

To take the t-system into consideration when evaluating the physiological significance of the G_M dynamics during AP firing for the sink membrane region during AP initiation, AP propagation, and t-system excitation, this study initially developed and calibrated appropriate linear circuit models for rat EDL muscle fiber in which the changes in G_M during AP firing were observed. This involved the comparison of electrophysiological recordings of passive membrane properties with the corresponding electrical properties of equivalent circuit models that either omitted or allowed for tubular morphology in the form of luminal resistance terms. The circuit models containing a t-system luminal resistance closely replicated experimental observations of frequency-dependent length constants and sinusoidal current propagation velocities. In contrast, in the absence of a t-system luminal resistance, predicted values markedly diverged from experimental observations even at frequencies slightly above DC.

Concordant predictions followed determinations of the conduction properties of the muscle fibers under study. AP conduction velocities were measured in rat EDL muscle as 1.92 ± 0.11 m s^{-1}. This velocity was matched by the passive velocity of a sinusoidal current of 410 ± 29 Hz. We termed this the "equivalent frequency" of the AP because the components of the circuit currents that convey AP propagation must be at least as fast as the AP itself. Fourier analysis of the AP waveform showed its median frequency to be 396 ± 15 Hz, close to this equivalent frequency. This suggested that about half of the power in the AP is contained in frequencies that conduct sufficiently fast to be important in AP propagation. Similarly, the passive conduction velocity of ∼400 Hz sine waves in the cable model containing a t-system luminal resistance matched the experimental AP velocity. In contrast, high frequencies (>1,200 Hz) were required to replicate the observed AP propagation velocities in models that did not contain tubular luminal resistances. Such frequencies were poorly represented in the AP waveform, suggesting that a significant t-system luminal resistance is required to explain the observed AP propagation velocity on the basis of the frequency content in the AP waveform.

The possible functional significance of such a t-system luminal resistance was next explored by convolution of the transfer functions describing the cable structures with either a 1-ms-long square current pulse or a recorded AP waveform. These analyses were limited to those portions of excitation and propagation through which the membrane showed linear behavior. Nevertheless, such an analysis predicted that the luminal resistance results in a steeper rise in electrotonic potential and a higher peak during a 1-ms square current pulse, as might occur during endplate activation. It similarly predicted a more rapid rate of voltage deflection at all distances from the point of an AP application while not affecting the magnitudes of such voltage changes. These outcomes were compatible with an effect of the luminal resistance in enhancing propagation velocity of APs. Such an effect of the t-system luminal resistance in enhancing sarcolemmal AP propagation velocity is confirmed in our companion paper using the nonlinear model (Fraser et al., 2011).

Finally, the analysis suggested that luminal resistances strongly influenced the nature of the t-system excitation. This was apparent from calculations of the voltage responses across the sarcolemmal membrane, the t-system membrane, and the luminal resistance at 100 µm from the site of application of a sarcolemmal voltage input in the form of an AP. Analysis of the frequency content of

the voltage changes across the sarcolemma, the t-system membrane, and t-system luminal resistance, through determination of their median frequencies, predicted that the voltage change across the t-system membrane predominantly contained low frequency components, whereas the voltage change across the luminal resistance contained a substantially higher frequency content. The luminal resistance thus would exert a low-pass–filtering effect preferentially admitting low rather than high frequency components of imposed currents to charge the t-system membrane. Higher frequencies would only affect the voltage across the luminal resistance and thereby became irrelevant for t-system excitation. This property of the t-system membrane, being charged by low rather than by high frequency components of the circuit currents, indicates that t-system excitation is likely to be highly dependent on its G_M, in contrast to a relative G_M independence of the higher frequency sarcolemmal currents.

To evaluate the functional role of the G_M dynamics in AP-firing fibers (Pedersen et al., 2009a,b), the present study computed the predicted voltage response of the distributed cable structure during the applications of a 1-ms square current pulse that mimicked an electrotonic endplate current or to AP waveforms that mimicked the voltage source that generates the circuit currents during AP propagation. G_M was adjusted to match the conditions in resting muscle fibers before AP firing; the Phase I G_M reduction at the onset of AP firing; and the Phase II, almost fivefold increase in G_M during prolonged AP firing.

This demonstrated that the Phase I G_M decrease would produce only minor increases in the electrotonic response to 1-ms square currents under normal resting conditions. However, when the baseline G_M was elevated to simulate either the larger expression level of ClC-1 channel at the endplate region (Papponen et al., 2005) or the elevated extracellular K^+ experienced in working muscle (Hník et al., 1976; Nielsen et al., 2003), the reduction in G_M during Phase I caused a substantial increase in sarcolemmal excitability. This analysis suggested that a reduction in G_M might enhance neuromuscular transmission in working muscle. The fivefold increase in G_M during Phase II reduced the voltage response to a 1-ms square current pulse by ~50% even under baseline conditions and was more pronounced at elevated $[K^+]$.

In contrast, the influence of G_M dynamics for sarcolemmal AP propagation was very limited. Neither the reduction in G_M during Phase I nor even the large increase in G_M during Phase II had substantial effects on the passive charging of the sink membrane region during AP propagation. This outcome was not markedly affected by elevating the extracellular K^+. These findings are consistent with the notion that AP propagation is conveyed by the high frequency components of the circuit currents because at such frequencies, the membrane transfer impedance becomes independent of G_M. Furthermore, these findings are compatible with the theoretical studies in un-myelinated axons (Hodgkin and Huxley, 1952; Noble, 1972) that suggest a minor role of G_M in membrane excitability and underline the fact that the filtering actions of the t-system luminal resistance enhance the physiological role of G_M in AP-firing muscle fibers.

Finally, the reduction in G_M during Phase I caused the passive voltage responses of the t-system membrane shells to a surface AP waveform to become larger and broader. Conversely, the large increase in G_M during Phase II markedly reduced the peaks of passive voltage responses and caused them to become narrower, such that the excitation of the deeper parts of the t-system was reduced by >80%. These effects of G_M changes during AP firing were more pronounced at elevated $[K^+]$. The profound influence of G_M upon t-system excitability results from the low-pass–filtering effect of the luminal resistance, as at low frequencies the membrane transfer impedance is considerably influenced by G_M.

Collectively, the findings of this study demonstrate and quantify a significant t-system luminal resistance in mammalian EDL muscle. They show that the influence of this resistance is to filter the AP waveform such that high frequency components are important for conduction of the sarcolemma AP, whereas low frequency components preferentially charge the t-system membranes. This frequency splitting ensures a high sarcolemmal conduction velocity as the higher frequency components of the AP avoid charging the t-system capacitance. It also ensures that G_M changes have markedly different influences on sarcolemmal and t-system excitation, such that surface AP propagation is little influenced by even large G_M changes, whereas t-system excitability is sharply influenced by G_M changes. Thus, the G_M decrease that occurs on AP firing is likely to enhance t-system and neuromuscular junction excitability. This is in accordance with experimental observations that Cl^- channel inhibition enhances t-system excitability (Pedersen et al., 2004). The large G_M increase that occurs after prolonged AP firing would cause significant reduction in t-system and neuromuscular junction excitability and is therefore likely to contribute significantly to the failure of excitation–contraction coupling in fatigue.

APPENDIX 1

Derivation of expressions for the equivalent impedances

In the three cable structures that were used in this study to represent the linear electrical properties of EDL muscle fibers, the equivalent impedances, Z_M, represented the sarcolemma and t-system membranes in addition to t-system luminal resistances. These equivalent impedances were characteristic for the particular circuits, and

each circuit therefore required separate derivations. In these derivations, the resistive components, R_M ($R_M = G_M^{-1}$), represent ion channels open at the resting membrane potential, and the parallel capacitative components, C_M, represent unit membrane dielectric properties. The impedance of a resistor (Z_R) and that of a capacitor (Z_C) are, respectively, given by:

$$Z_R = R, \tag{A1.1}$$

$$Z_C = 1/j2\pi fC, \tag{A1.2}$$

where R is resistance, C is capacitance, j is the imaginary operator, and f is the frequency, the independent variable in the frequency domain. Thus, the analytical solution for the equivalent impedance of unit membrane area of the simple cable structure ($Z_{M,Simple}$), a resistance and capacitance in parallel, (Fig. 2 A, left) was given by:

$$Z_{M,Simple} = \frac{R_M}{1+(\omega C_M R_M)^2} - j\frac{\omega C_M {R_M}^2}{1+(\omega C_M R_M)^2}. \tag{A1.3}$$

Note that $Z_{M,Simple}$ is a complex number, containing separate real and imaginary (j) parts. R_M represents the membrane resistance, and C_M represents the membrane capacitance, both of unit membrane area, and $\omega = 2\pi f$.

The lumped cable (Fig. 2 B, left) included an R_A term set to 10 or 20% of the DC membrane impedance to separate sarcolemmal from t-system parallel RC components. Its equivalent impedance ($Z_{M,Lumped}$) was determined as follows. First, the equivalent impedance for the parallel sarcolemma membrane resistance, $R_{M,S}$, and sarcolemma membrane capacitance, $C_{M,S}$, of unit surface membrane area was given by:

$$Z_{M,S} = \frac{R_{M,S}}{1+(\omega C_{M,S} R_{M,S})^2} - j\frac{\omega C_{M,S} R_{M,S}^2}{1+(\omega C_{M,S} R_{M,S})^2} = a_{M,S} - jb_{M,S}, \tag{A1.4}$$

where $a_{M,S}$ and $b_{M,S}$ represent the real and the imaginary parts of the equivalent impedance of the sarcolemma membrane, respectively. Then, the equivalent impedance for R_A, in series with the parallel membrane resistance, $R_{M,T}$, and membrane capacitance, $C_{M,T}$, of the t-system was given by:

$$Z_{M,T} = \frac{R_A + (\omega C_{M,T} R_{M,T})^2 R_A + R_{M,T}}{1+(\omega C_{M,T} R_{M,T})^2} - j\frac{\omega C_{M,T} R_{M,T}^2}{1+(\omega C_{M,T} R_{M,T})^2} = a_{M,T} - jb_{M,T}, \tag{A1.5}$$

where $a_{M,T}$ and $b_{M,T}$ represent the real and the imaginary parts of the equivalent impedance, respectively. The equivalent impedance for the entire lumped cable circuit was therefore given by

$$Z_{M,Lumped} = \frac{Z_{M,S} Z_{M,T}}{Z_{M,S} + Z_{M,T}} = A_M + jB_M, \tag{A1.6}$$

where A_M and B_M represent the real and the imaginary parts of the total equivalent impedance, respectively. These were, in turn, given by:

$$B_M = \frac{(b_{M,S}a_{M,T} + b_{M,T}a_{M,S})(a_{M,S} + a_{M,T}) + (a_{M,S}a_{M,T} - b_{M,S}b_{M,T})(b_{M,S} + b_{M,T})}{(a_{M,S} + a_{M,T})^2 + (b_{M,S} + b_{M,T})^2}. \tag{A1.7}$$

$$A_M = \frac{(a_{M,S}a_{M,T} - b_{M,S}b_{M,T})(a_{M,S} + a_{M,T}) + (b_{M,S}a_{M,T} + b_{M,T}a_{M,S})(b_{M,S} + b_{M,T})}{(a_{M,S} + a_{M,T})^2 + (b_{M,S} + b_{M,T})^2}, \tag{A1.8}$$

To calculate the equivalent impedance of the distributed cable structure, the membrane impedance of the surface membrane, $Z_{M,D,S}$, given by Eq. A1.4 was placed in parallel with the equivalent impedance of the t-system, $Z_{M,D,T}$. This was computed using Eqs. A1.6–A1.8:

$$Z_{M,Distributed} = \frac{Z_{M,D,S} Z_{M,D,T}}{Z_{M,D,S} + Z_{M,D,T}}. \tag{A1.9}$$

To find $Z_{M,D,T}$, the equivalent impedance of the membrane in the deepest t-system shell, $Z_{M,D,T,Eq.20}$, was determined using Eq. A1.3, and then added to the luminal resistance, $R_{l,20}$, that connected this shell to the second deepest shell, Eq. A1.5. The equivalent impedance of this sum was in parallel with the equivalent impedance of the membrane in the second deepest shell, $Z_{M,D,T,Eq.19}$, so the equivalent impedance of the membranes of both the deepest and the second deepest shells and the resistance separating the two membranes then could be calculated from:

$$Z_{M,D,T,Eq.20-19} = \frac{(Z_{M,D,T,Eq.20} + R_{l,20}) Z_{M,D,T,Eq.19}}{(Z_{M,D,T,Eq.20} + R_{l,20}) + Z_{M,D,T,Eq.19}}. \tag{A1.10}$$

$Z_{M,D,T,Eq.20-19}$ was then added to the resistance in front of the second deepest shell and so on throughout all the shells of the t-system.

Calculating the voltage drop across the membranes of the t-system in the distributed cable

In contrast to the calculations of the equivalent impedance of the t-system in the distributed cable, which was initiated from the deepest t-system shell, the voltage response across the membranes of the shells was started by

first finding the voltage division between the outermost luminal resistance and the equivalent impedance of the rest of the t-system structure. Once the voltage drop across the membrane of the first shell had been determined, another voltage division of this voltage between the luminal resistance that separated the first from the second shell and the equivalent impedance containing the membrane of the second shell and all deeper structures was performed. This procedure was continued down the t-system and can be summarized as follows:

$$V_{Z_{M,T,D,Eq.n+1}} = V_{Z_{M,T,D,Eq.n}} \frac{Z_{M,T,D,n+1}}{Z_{M,T,D,n+1} + R_{T,D,n+1}}. \quad \text{(A1.11)}$$

APPENDIX 2

Fourier transformations of circuit input

To obtain the frequency content of propagating APs and to simplify the mathematical procedures of convolution and circuit analysis, a large proportion of the calculations were performed in the frequency domain rather than in the time domain. Extracting the frequency content of propagating APs obtained from rat EDL muscle fibers (Fig. 3 A) involved their forward discrete Fourier transformation using the same Signal software system used for the experimental acquisition of data (see Materials and methods). The discrete Fourier transform $\mathrm{K}(\omega)$ is given by:

$$\mathrm{K}(\omega) = T\sum_{n=0}^{N-1} \kappa(t)\exp(-j\omega t). \quad \text{(A2.1)}$$

In Eq. A2.1, $\kappa(t)$ represents the experimentally recorded AP waveform, T is the inverse of the sampling frequency, N is the number of data points included in the analysis, and ω is the angular frequency, $2\pi f$, where f represents the frequency. The period of the first harmonic frequency corresponded to the duration of this sampling window. The program isolated real, $\mathrm{K}(\omega)_{real}$, and imaginary, $\mathrm{K}(\omega)_{imag}$, parts of the resulting frequency domain representation using the following equations:

$$\mathrm{K}(\omega)_{real} = T\sum_{n=0}^{N-1} \kappa(t)\cos(\omega t), \quad \text{(A2.2)}$$

$$\mathrm{K}(\omega)_{imag} = T\sum_{n=0}^{N-1} \kappa(t)\sin(\omega t). \quad \text{(A2.3)}$$

Two variants of this transformation could be performed. First, for the purposes of convolution analysis, the analysis was performed for integer multiples (0 to N-1) of the first harmonic frequency. Second, the Fourier transforms of the APs examined here were also examined along a logarithmic rather than a linear frequency scale to permit closer scrutiny of the lower frequencies to which attention is directed in this paper. This was possible in view of the AP records being time limited and accordingly assuming zero values beyond the duration of the AP waveform. Previous analyses (Huang, 1983) pointed out that they thus assume infinite periods and consequently possess Fourier transform values available as continuous rather than only discrete functions along the frequency abscissa. This contrasts with the situation for periodic stationary functions for which the discrete Fourier transform coefficients are only available at integer multiples of a fixed harmonic frequency corresponding to the inverse of the sampling period.

The inverse discrete Fourier transform

The final step in our analysis involved recovery of the voltage responses at the different distances along the cable structures as functions of time rather than frequency. This was achieved by inverse discrete Fourier transformation. Because the input functions of the sinusoidal currents or AP waveform were real, these outputs should also be real and therefore Hermitian and consequently symmetrical around the Nyquist frequency. However, the convolution consisted of a multiplication of the input function with the transfer function, which did not display a similar symmetrical behavior around the Nyquist frequency, rather decaying to zero at high frequencies. Accordingly, the inverse Fourier transform was performed from DC to the Nyquist frequency. To still include frequency components at the highest frequencies, the outputs were multiplied by 2, reflecting the symmetrical nature of a real function in the frequency domain (Bracewell, 1999):

$$\kappa(t) = 2f_1\sum_{n=0}^{N/2} \mathrm{K}(\omega)\exp(-j\omega t), \quad \text{(A2.4)}$$

where f_1 represents the first harmonic frequency. Inverse Fourier transforms normally contain a product of two complex numbers, which can result in a complex output in the time domain. However, for purely real data such as a propagating AP, the output of the inverse transform must also be real, implying that the imaginary part of the inverse transform is zero. Under these conditions, the inverse transform reduces to the readily determined real expression:

$$\kappa(t) = 2f_1\sum_{n=0}^{N/2} (\mathrm{K}(\omega)_{real}\cos(\omega t) - \mathrm{K}(\omega)_{imag}\sin(\omega t)), \quad \text{(A2.5)}$$

where $K(\omega)$ represents the experimental data in the frequency domain. Back-transformation of AP waveforms after such frequency domain analysis recovered the original waveform. The respective real and imaginary components of the Fourier transforms of the AP confirm that the features of these components were appropriate to those of the originating function in the time domain. Thus, the AP, being entirely real, is time limited, and takes zero value for $t < 0$. Correspondingly, the real and imaginary parts of the resulting Fourier transform, respectively, formed even and odd functions around the Nyquist frequency.

We acknowledge the Danish Medical Research Council (to T.H. Pedersen), the British Medical Research Council, the Wellcome Trust, and the British Heart Foundation for their generous support. J.A. Fraser acknowledges support from a Sir David Phillips Research Fellowship from the Biotechnology and Biological Research Council (UK) and from a Research Fellowship from Gonville and Caius College (Cambridge).

Christopher Miller served as editor.

Submitted: 3 August 2010
Accepted: 29 May 2011

REFERENCES

Adrian, R.H., and L.D. Peachey. 1973. Reconstruction of the action potential of frog sartorius muscle. *J. Physiol.* 235:103–131.

Adrian, R.H., W.K. Chandler, and A.L. Hodgkin. 1969a. The kinetics of mechanical activation in frog muscle. *J. Physiol.* 204:207–230.

Adrian, R.H., L.L. Costantin, and L.D. Peachey. 1969b. Radial spread of contraction in frog muscle fibres. *J. Physiol.* 204:231–257.

Albuquerque, E.X., and S. Thesleff. 1968. A comparative study of membrane properties of innervated and chronically denervated fast and slow skeletal muscles of the rat. *Acta Physiol. Scand.* 73:471–480.

Boyd, I.A., and A.R. Martin. 1959. Membrane constants of mammalian muscle fibres. *J. Physiol.* 147:450–457.

Bracewell, R.N. 1999. The Fourier Transform and Its Applications. Third edition. McGraw-Hill, New York. 616 pp.

Bryant, S.H., and A. Morales-Aguilera. 1971. Chloride conductance in normal and myotonic muscle fibres and the action of monocarboxylic aromatic acids. *J. Physiol.* 219:367–383.

Cullen, M.J., S. Hollingworth, and M.W. Marshall. 1984. A comparative study of the transverse tubular system of the rat extensor digitorum longus and soleus muscles. *J. Anat.* 138:297–308.

Dulhunty, A.F. 1984. Heterogeneity of T-tubule geometry in vertebrate skeletal muscle fibres. *J. Muscle Res. Cell Motil.* 5:333–347. doi:10.1007/BF00713111

Dulhunty, A.F., G. Carter, and C. Hinrichsen. 1984. The membrane capacity of mammalian skeletal muscle fibres. *J. Muscle Res. Cell Motil.* 5:315–332. doi:10.1007/BF00713110

Eisenberg, R.S. 1983. Impedance Measurement of the Electrical Structure of Skeletal Muscle. *In* Handbook of Physiology, Section 10: Skeletal Muscle. L.D. Peachey, editor. American Physiological Society, Bethesda, MD. 301–323.

Falk, G., and P. Fatt. 1964. Linear electrical properties of striated muscle fibres observed with intracellular electrodes. *Proc. R. Soc. Lond. B Biol. Sci.* 160:69–123. doi:10.1098/rspb.1964.0030

Fink, R., and H.C. Lüttgau. 1976. An evaluation of the membrane constants and the potassium conductance in metabolically exhausted muscle fibres. *J. Physiol.* 263:215–238.

Fraser, J.A., C.L.-H. Huang, and T.H. Pedersen. 2011. Relationships between resting conductances, excitability, and t-system ionic homeostasis in skeletal muscle. *J. Gen. Physiol.* 138:95–116.

Gage, P.W., and R.S. Eisenberg. 1969. Action potentials, afterpotentials, and excitation–contraction coupling in frog sartorius fibers without transverse tubules. *J. Gen. Physiol.* 53:298–310. doi:10.1085/jgp.53.3.298

Hník, P., M. Holas, I. Krekule, N. Küriz, J. Mejsnar, V. Smiesko, E. Ujec, and F. Vyskocil. 1976. Work-induced potassium changes in skeletal muscle and effluent venous blood assessed by liquid ion-exchanger microelectrodes. *Pflugers Arch.* 362:85–94. doi:10.1007/BF00588685

Hodgkin, A.L. 1937. Evidence for electrical transmission in nerve: part I. *J. Physiol.* 90:183–210.

Hodgkin, A.L., and A.F. Huxley. 1952. A quantitative description of membrane current and its application to conduction and excitation in nerve. *J. Physiol.* 117:500–544.

Hodgkin, A.L., and B. Katz. 1949. The effect of sodium ions on the electrical activity of giant axon of the squid. *J. Physiol.* 108:37–77.

Hodgkin, A.L., and W.A. Rushton. 1946. The electrical constants of a crustacean nerve fibre. *Proc. R. Soc. Med.* 134:444–479.

Huang, C.L. 1983. Time domain spectroscopy of the membrane capacitance in frog skeletal muscle. *J. Physiol.* 341:1–24.

Huang, C.L. 1988. Intramembrane charge movements in skeletal muscle. *Physiol. Rev.* 68:1197–1247.

Huang, C.L., and L.D. Peachey. 1989. Anatomical distribution of voltage-dependent membrane capacitance in frog skeletal muscle fibers. *J. Gen. Physiol.* 93:565–584. doi:10.1085/jgp.93.3.565

Huang, C.L., and L.D. Peachey. 1992. A reconstruction of charge movement during the action potential in frog skeletal muscle. *Biophys. J.* 61:1133–1146. doi:10.1016/S0006-3495(92)81923-9

Koch, M.C., K. Steinmeyer, C. Lorenz, K. Ricker, F. Wolf, M. Otto, B. Zoll, F. Lehmann-Horn, K.H. Grzeschik, and T.J. Jentsch. 1992. The skeletal muscle chloride channel in dominant and recessive human myotonia. *Science.* 257:797–800. doi:10.1126/science.1379744

Kwieciński, H., F. Lehmann-Horn, and R. Rüdel. 1984. The resting membrane parameters of human intercostal muscle at low, normal, and high extracellular potassium. *Muscle Nerve.* 7:60–65. doi:10.1002/mus.880070110

Macdonald, W.A., T.H. Pedersen, T. Clausen, and O.B. Nielsen. 2005. *N*-Benzyl-*p*-toluene sulphonamide allows the recording of trains of intracellular action potentials from nerve-stimulated intact fast-twitch skeletal muscle of the rat. *Exp. Physiol.* 90:815–825. doi:10.1113/expphysiol.2005.031435

McComas, A.J., and K. Mrozek. 1968. The electrical properties of muscle fiber membranes in dystrophia myotonica and myotonia congenita. *J. Neurol. Neurosurg. Psychiatry.* 31:441–447. doi:10.1136/jnnp.31.5.441

Nielsen, J.J., M. Kristensen, Y. Hellsten, J. Bangsbo, and C. Juel. 2003. Localization and function of ATP-sensitive potassium channels in human skeletal muscle. *Am. J. Physiol. Regul. Integr. Comp. Physiol.* 284:R558–R563.

Nielsen, O.B., F. de Paoli, and K. Overgaard. 2001. Protective effects of lactic acid on force production in rat skeletal muscle. *J. Physiol.* 536:161–166. doi:10.1111/j.1469-7793.2001.t01-1-00161.x

Noble, D. 1972. The relation of Rushton's 'liminal length' for excitation to the resting and active conductances of excitable cells. *J. Physiol.* 226:573–591.

Padmanabhan, N., and C.L. Huang. 1990. Separation of tubular electrical activity in amphibian skeletal muscle through temperature change. *Exp. Physiol.* 75:721–724.

Papponen, H., T. Kaisto, V.V. Myllylä, R. Myllylä, and K. Metsikkö. 2005. Regulated sarcolemmal localization of the muscle-specific ClC-1 chloride channel. *Exp. Neurol.* 191:163–173. doi:10.1016/j.expneurol.2004.07.018

Peachey, L.D. 1965. The sarcoplasmic reticulum and transverse tubules of the frog's sartorius. *J. Cell Biol.* 25:209–231. doi:10.1083/jcb.25.3.209

Pedersen, T.H., O.B. Nielsen, G.D. Lamb, and D.G. Stephenson. 2004. Intracellular acidosis enhances the excitability of working muscle. *Science.* 305:1144–1147. doi:10.1126/science.1101141

Pedersen, T.H., F. de Paoli, and O.B. Nielsen. 2005. Increased excitability of acidified skeletal muscle: role of chloride conductance. *J. Gen. Physiol.* 125:237–246. doi:10.1085/jgp.200409173

Pedersen, T.H., F.V. de Paoli, J.A. Flatman, and O.B. Nielsen. 2009a. Regulation of ClC-1 and K_{ATP} channels in action potential–firing fast-twitch muscle fibers. *J. Gen. Physiol.* 134:309–322. doi:10.1085/jgp.200910290

Pedersen, T.H., W.A. Macdonald, F.V. de Paoli, I.S. Gurung, and O.B. Nielsen. 2009b. Comparison of regulated passive membrane conductance in action potential–firing fast- and slow-twitch muscle. *J. Gen. Physiol.* 134:323–337. doi:10.1085/jgp.200910291

Pusch, M. 2002. Myotonia caused by mutations in the muscle chloride channel gene CLCN1. *Hum. Mutat.* 19:423–434. doi:10.1002/humu.10063

Schneider, M.F. 1970. Linear electrical properties of the transverse tubules and surface membrane of skeletal muscle fibers. *J. Gen. Physiol.* 56:640–671. doi:10.1085/jgp.56.5.640

Sheikh, S.M., J.N. Skepper, S. Chawla, J.I. Vandenberg, S. Elneil, and C.L. Huang. 2001. Normal conduction of surface action potentials in detubulated amphibian skeletal muscle fibres. *J. Physiol.* 535:579–590. doi:10.1111/j.1469-7793.2001.t01-1-00579.x

Stephenson, D.G. 2006. Tubular system excitability: an essential component of excitation-contraction coupling in fast-twitch fibres of vertebrate skeletal muscle. *J. Muscle Res. Cell Motil.* 27:259–274. doi:10.1007/s10974-006-9073-6

Valdiosera, R., C. Clausen, and R.S. Eisenberg. 1974a. Circuit models of the passive electrical properties of frog skeletal muscle fibers. *J. Gen. Physiol.* 63:432–459. doi:10.1085/jgp.63.4.432

Valdiosera, R., C. Clausen, and R.S. Eisenberg. 1974b. Impedance of frog skeletal muscle fibers in various solutions. *J. Gen. Physiol.* 63:460–491. doi:10.1085/jgp.63.4.460

Valdiosera, R., C. Clausen, and R.S. Eisenberg. 1974c. Measurement of the impedance of frog skeletal muscle fibers. *Biophys. J.* 14:295–315. doi:10.1016/S0006-3495(74)85917-5

Wallinga, W., S.L. Meijer, M.J. Alberink, M. Vliek, E.D. Wienk, and D.L. Ypey. 1999. Modelling action potentials and membrane currents of mammalian skeletal muscle fibres in coherence with potassium concentration changes in the T-tubular system. *Eur. Biophys. J.* 28:317–329. doi:10.1007/s002490050214